



# The underappreciated importance of solar radiation in constraining spring phenology of temperate ecosystems in the Northern and Eastern United States



Yating Gu<sup>a</sup>, Yingyi Zhao<sup>a</sup>, Zhengfei Guo<sup>a</sup>, Lin Meng<sup>b</sup>, Kun Zhang<sup>a</sup>, Jing Wang<sup>a,c</sup>,  
Calvin K.F. Lee<sup>a</sup>, Jing Xie<sup>d</sup>, Yantian Wang<sup>e</sup>, Zhengbing Yan<sup>a,f</sup>, He Zhang<sup>a</sup>, Jin Wu<sup>a,g,\*</sup>

<sup>a</sup> Research Area of Ecology and Biodiversity, School of Biological Sciences, The University of Hong Kong, Pokfulam, Hong Kong, China

<sup>b</sup> Department of Earth and Environmental Sciences, Vanderbilt University, Nashville, USA

<sup>c</sup> School of Ecology, Sun Yat-Sen University, Guangzhou 510275, China

<sup>d</sup> School of Geography and Planning, Sun Yat-Sen University, Guangzhou, China

<sup>e</sup> College of Resources and Environment, University of Chinese Academy of Sciences, Beijing 100049, China

<sup>f</sup> State Key Laboratory of Vegetation and Environmental Change, Institute of Botany, Chinese Academy of Sciences, Beijing, China

<sup>g</sup> Institute for Climate and Carbon Neutrality, The University of Hong Kong, Hong Kong, China

## ARTICLE INFO

Edited by Jing M. Chen

**Keywords:**

Land surface phenology  
Leaf unfolding date  
Trophic interactions  
Climate feedback  
Optimized trade-off strategy  
Optimal photosynthesis gain

## ABSTRACT

Spring phenology of temperate ecosystems is highly sensitive to climate change, generating various impacts on many important terrestrial surface biophysical processes. Although various prognostic models relying on environmental variables of temperature and photoperiod have been developed for spring phenology, comprehensive ecosystem-scale evaluations over large landscapes and long-time periods remain lacking. Further, environmental variables other than temperature and photoperiod might also importantly constrain spring phenology modelling but remain under-investigation. To address these issues, we leveraged around 20-years datasets of environmental variables (from Daymet and GLDAS products) and the spring phenology metric (i.e., the greenup date) respectively derived from MODIS and PhenoCams across 108 sites in the Northern and Eastern United States. We firstly cross-compared MODIS-derived greenup date with official PhenoCams product with high accuracy ( $R^2 = 0.70$ ). Then, we evaluated the three prognostic models (i.e., Growing Degree Date (GDD), Sequential (SEQ) and optimality-based (OPT)) with MODIS-derived spring phenology, assessed the model residuals and their associations with soil moisture, rainfall, and solar radiation, and revised the two photoperiod-relevant models (SEQ, OPT) by replacing the daylength variable with solar radiation, which was found to contribute the most to model residuals. We found that 1) all models demonstrated good capability in characterizing spring phenology, with OPT performing the best ( $\text{RMSE} = 8.04 \pm 5.05$  days), followed by SEQ ( $\text{RMSE} = 10.57 \pm 7.77$  days) and GDD ( $\text{RMSE} = 10.84 \pm 8.42$  days), 2) all models displayed high model residuals showing tight correlation with solar radiation ( $r = 0.45\text{--}0.75$ ), and 3) the revised models that included solar radiation significantly performed better with an RMSE reduction by 22.08%. Such results are likely because solar radiation better constrains early growing season plant photosynthesis than photoperiod, supporting the hypothesis of spring phenology as an adaptive strategy to maximize photosynthetic carbon gain (approximated by solar radiation) while minimizing frost damage risk (captured by temperature). Collectively, our study reveals the underappreciated importance of solar radiation in constraining spring phenology of temperate ecosystems, and suggests ways to improve spring phenology modelling and other phenology-related ecological processes.

## 1. Introduction

In the temperate ecosystems, spring phenology, which has been

advanced in response to recent global warming, is widely used as a diagnostic tool for Earth's surface energy balance and net ecosystem carbon exchange processes (Piao et al., 2019). For instance, spring

\* Corresponding author at: School of Biological Sciences, The University of Hong Kong, Pokfulam Road, Hong Kong, China.  
E-mail address: [jinwu@hku.hk](mailto:jinwu@hku.hk) (J. Wu).

phenology regulates many important terrestrial surface biophysical processes, including land surface albedo (Lin et al., 2022; Zhang et al., 2017), spring carbon assimilation (Lee and Ibáñez, 2021), and annual biomass growth (Mäkitalo et al., 2018). Furthermore, spring phenology not only affects many phenology-associated biotic interactions, such as interspecies competition and interactions with other organisms (Chmura et al., 2019), but also the climate feedbacks mediated by vegetation, such as earlier soil water depletion and subsequent increase in summer drought risks (Lian et al., 2020). Despite its important role in many ecological and earth surface processes, accurate mechanistic understanding and modelling of what drives the spring phenology variability over large vegetated ecosystems and long-time periods remain incomplete, resulting in large uncertainty in projecting future climate change impacts on spring phenology and other phenology-related ecological processes (Caparros-Santiago et al., 2021).

For a long time, spring phenology (indicated by the stages of leaf development) has been mechanistically connected with several key phenophases, such as endodormancy (dormancy because of physiological growth arresting), ecodormancy (dormancy due to unfavourable environmental conditions) (Lundell et al., 2020), and the active growth period (Savage and Chuine, 2021; Singh et al., 2017). Many studies suggest that various environmental factors, such as temperature and photoperiod, can affect the occurrence and development of these phenophases. Specifically, the favourable forcing temperature together with longer photoperiod in the active growth period accelerates the development rate of buds (Piao et al., 2019; Viherä-Aarnio et al., 2014). However, growth ceases when chilling begins to accumulate, and the photoperiod becomes shorter in autumn. These unsupportive environmental conditions ultimately cause leaf fall, which marks the start of the endodormancy period (Schwartz and Hanes, 2010; Tang et al., 2016). After enduring the chilling effect and meeting the forcing requirement, perceptible changes in ambient environmental conditions begin to shape, enlarge, and open the buds in the ecodormancy period (Chuine et al., 2016; Fernandez et al., 2022). Accompanying these explorations on the proximate environmental cues on spring phenology regulation, many quantitative tools, such as the prognostic models of spring phenology that consider various phenophases and include forcing, chilling and photoperiod as model inputs, have also been developed (Basler, 2016; Shen et al., 2022; Wang et al., 2022). Depending on key phenophases and environmental factors being considered, these prognostic models normally include temperature-dependent models, such as Growing Degree Days (GDD) (De Réaumur, 1735; Dong et al., 2019; Zhou and Wang, 2018), endodormancy and ecodormancy in sequential relationships such as Sequential (SEQ) models (Ashcroft et al., 1974; Viswanathan et al., 2022), as well as endodormancy and ecodormancy in parallel relationships coupling the photoperiod effect, such as optimality-based (OPT) models (Meng et al., 2021b). However, other than temperature and photoperiod captured by the existing models, whether and how other environmental factors (e.g., precipitation (Fu et al., 2021; Yun et al., 2018), soil moisture (Fu et al., 2016), and solar radiation (Descals et al., 2022)) play a role in mediating spring phenology variability remains under-investigation.

To examine the validity of the key mechanisms underlying these prognostic models and to assess their accuracy in modelling spring phenology with climate change, many experimental and observational studies have been conducted. Currently, most model evaluations were conducted at the organism level. These evaluations mostly relied on either long-term in-situ observations of certain plant individuals or species (Flynn and Wolkovich, 2018; Roberts et al., 2015), or using experimental approaches that investigate the same plant species under different environmental conditions (Hänninen et al., 2019; Liu et al., 2011). Further, to explore the phenological sensitivity response to the continued global warming, scientists (Zhao et al., 2021; Zohner et al., 2020a) used prognostic models for future projections under various climate change scenarios. Despite considerable progress being made at the organism/species level, whether similar mechanisms/models can be

extended to the ecosystem level is unknown. An ecosystem-level assessment is critical, as the degree to which climate change will hamper the stability and persistence of ecosystem phenology remains largely an open question (Ovaskainen et al., 2013). Meanwhile, the forest ecosystem is made of tree individuals that often display large plasticity across both intra- and inter-specific levels in terms of their phenological sensitivity response to climate change (Fu et al., 2015; Peng et al., 2021; Tumajer et al., 2021). As a result, the ecosystem is more complex than any single individual organism/species, and the phenological knowledge we learnt from the organism level can not necessarily be directly transferable to the ecosystem level.

The recent increasing availability of long-time series remote sensing observations from both satellite and ground PhenoCam networks offers a timely opportunity to evaluate these prognostic models and associated mechanisms underneath these models at the ecosystem level. Satellite remote sensing has demonstrated its effectiveness in monitoring land surface phenology (LSP) by offering data covering large spatial extents with high temporal resolution over decadal time series (Bolton et al., 2020; Liu et al., 2015). In addition, relevant LSP products from satellites have also been generated and verified with free access, such as MCD12Q2 (Friedl et al., 2019) and VNP22Q2 (Zhang et al., 2020a) at a 500 m resolution. PhenoCam sensors provide continuous daily images that aid accurate monitoring of both fine and ecosystem-scale plant phenology for each plant functional type (Richardson et al., 2018a; Seyednasrollah et al., 2019). The accumulation of these remote sensing data improves both spatial and temporal monitoring of plant phenology and provides us great opportunities to assess phenology models and their mechanisms at the ecosystem level. Lastly, because satellite data can provide LSP monitoring in a consistent, continuous manner across both large spatial and temporal extents, especially relative to the PhenoCam means, it thus makes the satellite-based LSP a more preferable, scalable option for prognostic model assessments.

The large environmental gradients present in the temperate vegetated ecosystems of the Northern and Eastern United States provide a unique testbed to evaluate the application of state-of-the-art prognostic models in temperate areas, and to assess the effect of environmental variables, beyond chilling, forcing and photoperiod, on the modulation of spring phenology variability. Here we aim to answer the following questions: (1) To what extent can these prognostic models capture spring phenology in temperate ecosystems in the United States? (2) What environmental variable(s) dominantly regulate spring phenology but are not yet captured by current prognostic models? (3) Could revised prognostic models that include the missing environmental cues, as revealed in question (2), improve spring phenology modelling, and if so, what is the likely underlying mechanism? To address these questions, we selected all sites in the Northern and Eastern United States with paired measurements of satellite and PhenoCam phenology and environmental datasets. We trained and evaluated the three prognostic models of GDD, SEQ, and OPT for modelling spring phenology. Next, we analysed the relationships between the model residuals and each of the three environmental variables (i.e., preseason shortwave radiation ( $SR_{pre}$ ), preseason precipitation ( $P_{pre}$ ), and preseason soil moisture ( $SM_{pre}$ )) that have been previously connected with spring phenology of temperate ecosystems (Piao et al., 2022; Tao et al., 2020a) to assess whether other environmental variables that are not represented in the current prognostic models also importantly regulate spring phenology variability. Once an environmental variable (such as solar radiation) was found to contribute the most to model residuals, we revised the two photoperiod-relevant models (SEQ, OPT) by replacing the daylength variable with solar radiation and investigated whether the revised models could improve the model performance.

## 2. Study sites, materials, and methods

### 2.1. Study sites

In this study, we selected 108 sites that span large latitudinal and longitudinal ranges (Fig. 1). These sites encompass a range of plant functional types (PFTs), including deciduous broadleaf (DBF), grassland (GRA), and mixed forests (MXF). We selected these sites for three reasons. First, they are all distributed in temperate regions which are defined by the boundary of the level I Ecoregion 5 Northern Forests and Ecoregion 8 Eastern Temperate Forests by the United States Environmental Protection Agency (McMahon et al., 2001; Omernik, 1987). Second, the sites are mainly distributed in temperature-sensitive regions where are characterized as typical humid continental, or humid oceanic climate, and cover large environmental gradients, providing a unique dataset for comprehensive model evaluations over large landscapes. Notably, the distribution of annual precipitation is not uniform across these sites. The mean annual precipitation of 2001–2019 decreases from over 684 mm in the southern sites to about 17 mm in the northern sites, with most of the precipitation concentrated from May to August. While the mean annual temperature of 2001–2019 ranges from  $-2.51$  to  $24.25$  °C, the maximum summer temperature exceeds  $34.33$  °C and the minimum winter temperature can reach  $-38.77$  °C. Third, all the selected sites have both local phenology records from PhenoCam and LSP from satellite observations, which makes the PhenoCam-satellite cross-validation feasible.

### 2.2. Materials

We utilized several remote sensing data resources, including near-surface PhenoCam observations, LSP metrics derived from the

satellite-based MCD12Q2 product of Moderate Resolution Imaging Spectroradiometer (MODIS), as well as key environmental variables obtained either from remote sensing reanalysis data such as Daymet/GLDAS or via the Google Earth Engine platform.

#### 2.2.1. PhenoCam data and associated phenological metrics

We used the latest PhenoCam Dataset v2.0, which was organized and processed by Seyednasrollah et al. (2019), for two reasons. First, digital repeat photography, along with the Green Chromatic Coordinate (GCC), provides an accurate and quantitative means for monitoring plant phenology (Brown et al., 2016; Caparros-Santiago et al., 2021), which can subsequently be used as “ground truth” to evaluate satellite-derived LSP. Second, the PhenoCam Dataset v2.0 employs a standardized approach to preprocess the data across all selected sites in a consistent way with provided GCC metric on a daily basis and official phenometrics to indicate key transition dates on an annual basis, which helps to reduce uncertainties associated with data preprocessing and phenology extractions from PhenoCams (Moon et al., 2021a).

We first extracted the timing of leaf unfolding date (LUD) from the official PhenoCam v2.0 dataset ([https://daac.ornl.gov/VEGETATION/guides/PhenoCam\\_V2.html](https://daac.ornl.gov/VEGETATION/guides/PhenoCam_V2.html); Seyednasrollah et al., 2019) using the metric rising\_transition\_25, which represents the transition date for the “greenness rising” stage that corresponds to 25.0% of the GCC amplitude of that stage. This metric has been widely used in previous studies to indicate LUD (Hufkens et al., 2018). As an independent evaluation on the reliability of this metric, we then derived our own phenometric to indicate LUD using a double logistic function algorithm proposed by (Elmore et al., 2012) with daily GCC time-series as input, and cross-compared our derived LUD records with the rising transition 25 metric provided by PhenoCam v2.0. Our analysis in Fig. S1 demonstrates that the two versions of LUD are overall very comparable, and

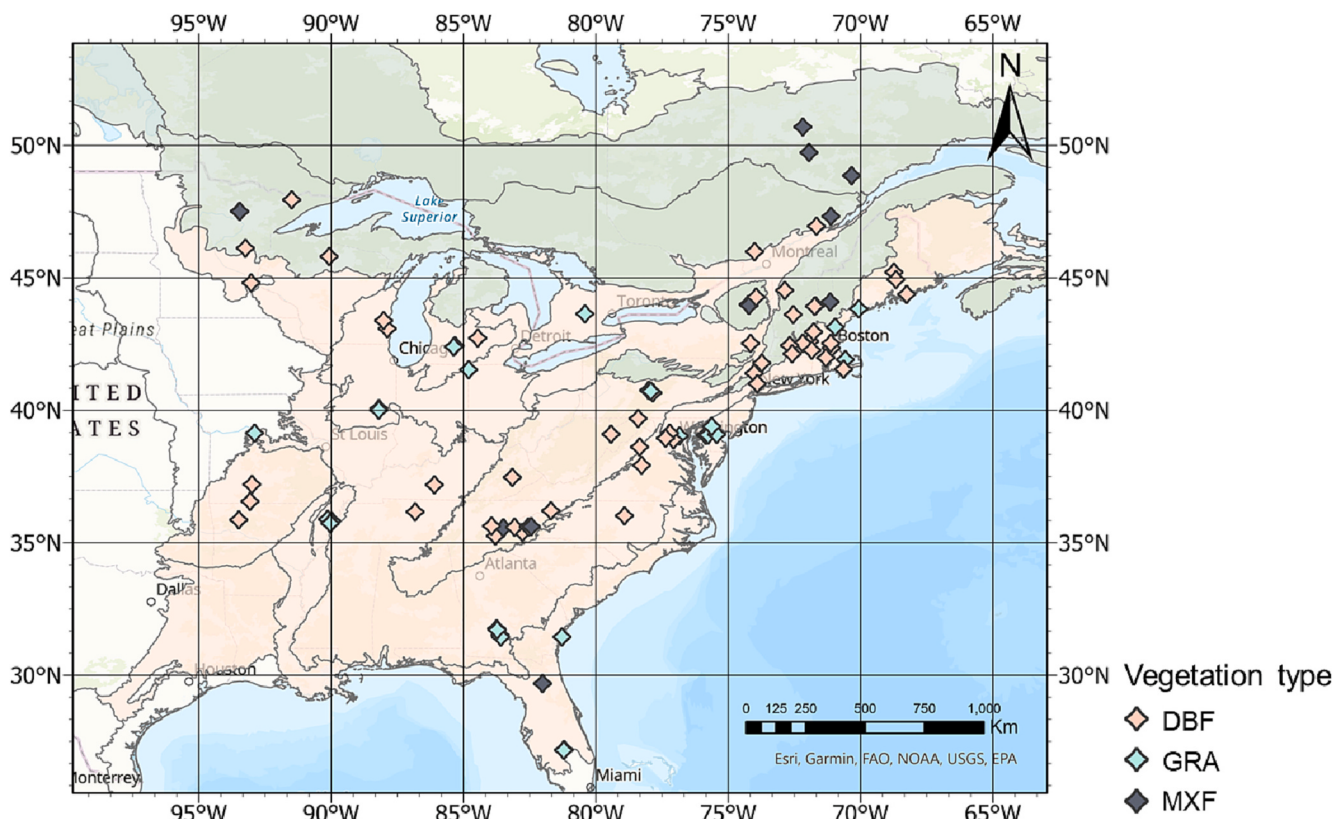


**Fig. 1.** Locations of study sites with both PhenoCam and satellite measurements. These study sites are within the level I Ecoregion 5 Northern Forests (aqua area) and Ecoregion 8 Eastern Temperate Forests (hermosa pink area) by the United States Environmental Protection Agency, and include three plant functional types of deciduous broadleaf (DBF), grassland (GRA), and mixed forests (MXF). (For interpretation of the references to colour in this figure legend, the reader is referred to the web version of this article.)

both show strong agreement with MODIS-derived LUD (details below), suggesting that the MODIS product is reasonably accurate for spring phenology monitoring.

### 2.2.2. MODIS-based LSP metrics

We extracted the 500 m resolution phenometrics from Collection 6 MODIS Land Cover Dynamics product MCD12Q2, covering the period from 2001 to 2019 (Friedl et al., 2019). This product was derived from the time-series of a 2-band Enhanced Vegetation Index (EVI2) calculated from MODIS Nadir Bidirectional Reflectance Distribution Function (BRDF)-Adjusted Reflectance (NBAR). The product includes six key phenological metrics (i.e., Greenup, MidGreenup, Maturity, Senescence, MidGreendown, and Dormancy), as well as quality layers for the derived phenological metrics (i.e., QA\_Detailed). This product was used for three reasons. First, it has a much longer time series compared with other phenological products such as VNP22Q2 (Zhang et al., 2020a), which has a temporal extent from 2013 to the present. Second, it has global coverage with a spatial resolution of 500 m, offering us the possibility to examine the ecosystem-level spring phenology variability. Thirdly, this phenometrics product has been rigorously evaluated previously with demonstrated accurate validation results across diverse forest ecosystems and over interannual timescales (Gonsamo and Chen, 2016; Peng et al., 2017; Xin et al., 2015; Fig. S1), thereby allowing for the comparison of phenological metrics across different sites and years. Notably, we used the satellite-derived Greenup (indicating the date when EVI2 first crossed 15.0% of the segment EVI2 magnitude; Friedl et al., 2019) to indicate spring phenology, or LUD. In order to derive the high quality LUD from the MCD12Q2 product, we conducted further data quality assessment including two steps. First, we turned to the quality assessment bands QA\_Detailed provided by the MCD12Q2 product (0: best; 1: good; 2: fair; 3: poor), retained only records that belonged to the ‘best’ or ‘good’ categories, and then used the average of all the remaining valid values of the neighboring  $3 \times 3$  pixels for the targeted site-year (Moon et al., 2022). Second, for each site with around 20-years LUD records, we interactively calculated the associated mean and standard deviation (std), and then used mean  $\pm 5 \times \text{std}$  to filter outliers. After quality control, we evaluated the accuracy of satellite-derived LUD data with the corresponding transition\_25 metric provided by PhenoCam v2.0 as the benchmark. Our analysis revealed that the transition\_25 metric and MODIS-derived LUD exhibited high agreement (Fig. S1a;  $R^2 = 0.70$ ), indicating that MODIS-derived LUD is a reliable spring phenology metric that can be used for subsequent evaluation of prognostic models.

### 2.2.3. Environmental data

We extracted spatially and temporally consistent meteorological data from the Daymet dataset (<https://daymet.ornl.gov>; Thornton et al., 2021). The dataset was generated by integrating ground observations with statistical modelling techniques for interpolation and extrapolation, and has demonstrated high accuracy (Thornton et al., 2017; Thornton et al., 2016). The dataset has a daily time step and 1 km spatial resolution for the period from 1980 to the present. Specifically, we used the online Fixed Sites Subsets Tool: Product - DAYMET platform (<https://modis.ornl.gov/sites/?list=all&product=Daymet>) to extract all key meteorological variables from 2001 to 2019 for each site, including daily maximum ( $T_{\max}$ ) and minimum ( $T_{\min}$ ) 2-m air temperature, daily total precipitation ( $P$ ), shortwave radiation ( $SR$ ), and daylength ( $DL$ ). Since Daymet does not include soil moisture in its records, we turned to another source for extracting soil moisture data from the GLDAS-2.1 dataset and converted the provided 3-h temporal resolution data into daily soil moisture, which we did on Google Earth Engine. The soil moisture data was subsequently resampled from the original 27.83 km resolution to a 1 km resolution to match with other environmental variables using the nearest neighbor approach.

Notably, the Daymet dataset only provides the variables of daily  $T_{\max}$  and  $T_{\min}$ . We then followed the method of (Zohner et al., 2020c) and used a sign curve function (Eq. (1)) to simulate the hourly temperature

( $T_{hour}$ ) of the day ( $time_{day}$ ) based on the provided  $T_{\max}$  and  $T_{\min}$ . With these simulated  $T_{hour}$  values, we finally derived daily mean temperature ( $T_{mean}$ ) using the mean of all 24  $T_{hour}$  values of that day.

$$T_{hour} = \frac{(T_{\max} - T_{\min})}{2} \times \sin\left(\frac{\pi}{12} \times time_{day} - \frac{\pi}{2}\right) + \frac{(T_{\max} + T_{\min})}{2} \quad (1)$$

## 2.3. Methods

### 2.3.1. Prognostic models

Three prognostic models were examined in this study, including GDD, SEQ, and OPT, illustrated below.

**2.3.1.1. The GDD model.** GDD is a one-phase model that only considers the ecodormancy period (De Réaumur, 1735; Hänninen 2016). The theory underlying this model is that many chemical reaction rates are temperature-dependent when constructing the cellular structure of leaf tissues (Johnson and Thornley, 1985). As such, LUD is hypothesized and modelled to be driven by the effective accumulated forcing that shows a direct link with plants' growing temperature, and LUD only occurs on the date  $t_1$  when the sum of the daily forcing state  $GDD(t)$  (Eq. (2)) exceeds a critical value  $GDD_C$ .

$$GDD(t) = \sum_{t_0}^{t_1} \max(T_t - T_{base}, 0), \text{ when } GDD(t) \geq GDD_C \quad (2)$$

Where  $T_t$  is the daily mean temperature,  $T_{base}$  is the base temperature often set 5 °C (Wang et al., 2020b),  $t_0$  (set as January 1st of each calendar year (Wang et al., 2020b)) and  $t_1$  are the start date and end date to calculate GDD, respectively, and  $GDD_C$  is a site/ecoregion-specific parameter that was calibrated from the time-series data.

**2.3.1.2. The Sequential model.** SEQ was developed because the temperature effect on spring phenology could be further divided into winter chilling and spring forcing (Cannell and Smith, 1983; Hänninen et al., 2019; Körner and Basler, 2010), which are respectively connected to endodormancy and ecodormancy periods (Chuine et al., 2016). Meanwhile, daylength (or photoperiod), a proxy of accumulated sunlight over the full day and showing direct link with the plant's active growth rates once leaf onset occurs, is another important environmental trigger for spring phenology (Meng et al., 2021b; Way and Montgomery, 2015; Zohner et al., 2016). Based on these, SEQ was proposed, in which both dormancy periods (endodormancy and ecodormancy) were considered, respectively captured by chilling and forcing, along with subsequent active growth period, captured by daylength.

In SEQ, the chilling response can be described using a triangular function of Eq. (3) (Zhang et al., 2018). Here,  $T_{\min}$ ,  $T_{\text{opt}}$  and  $T_{\max}$  indicate the minimal, optimal, and maximum chilling temperature, respectively, and  $T_t$  indicates the daily mean temperature on date  $t$ . To represent the forcing effect, we followed (Basler, 2016) and used Eqs. (4)–(6) for simulating the forcing effect. The general idea is to use the daylength  $DL(t)$  to approximate the forcing effect (Eq. (4)), and forcing only occurs when the accumulated chilling requirement has been met (i.e., beyond the critical value  $C_{req}$ ) (Eqs. (5)–(6)). Finally, LUD occurs on the date  $t_1$  when the sum of daily forcing state  $S_f(t)$  (Eq. (7)) exceeds a critical value  $F_{\text{crit}}$ .

$$R_c(t) = \begin{cases} \frac{T_t - T_{\min}}{T_{\text{opt}} - T_{\min}}, & T_{\min} \leq T_t < T_{\text{opt}} \\ \frac{T_t - T_{\text{opt}}}{T_{\max} - T_{\text{opt}}}, & T_{\text{opt}} \leq T_t < T_{\max} \\ 0, & \text{if } T_t < T_{\min} \text{ or } T_t > T_{\max} \end{cases} \quad (3)$$

$$R_f(t) = \left( \frac{DL(t)}{24} \right)^k \bullet \max(T_t - T_{base}, 0) \quad (4)$$

$$k = \begin{cases} 0, & S_c(t) < C_{\text{req}} \\ 1, & S_c(t) \geq C_{\text{req}} \end{cases} \quad (5)$$

$$S_c(t) = \sum_{t_0}^{t_1} R_c(t) \quad (6)$$

$$S_f(t) = \sum_{t_0}^{t_1} R_f(t), \text{ when } S_f(t) \geq F_{\text{crit}} \quad (7)$$

Where:  $R_c(t)$  and  $R_f(t)$  indicate the states of chilling and forcing on date  $t$ , and  $S_c(t)$  and  $S_f(t)$  indicate the accumulated chilling and forcing since  $t_0$  (set as January 1st of each year) to  $t_1$ ;  $T_{\text{base}}$  ( $= 5^\circ\text{C}$ ),  $T_{\min}$  ( $= -5^\circ\text{C}$ ),  $T_{\text{opt}}$  ( $= 10^\circ\text{C}$ ), and  $T_{\max}$  ( $= 25^\circ\text{C}$ ) are set as empirical constants following (Wang et al., 2020b); The model has two parameters to be fitted, including  $C_{\text{req}}$  and  $F_{\text{crit}}$ .

**2.3.1.3. The optimality-based model.** OPT was developed based on the eco-evolutionary optimality principle (Meng et al., 2021b), in which it hypothesizes spring phenology as an optimal strategy for plants to maximize photosynthetic carbon gain (e.g., approximated by photoperiod and forcing) while minimizing frost damage risk (e.g., captured by chilling) (Fu et al., 2019; Körner, 2006; Richardson et al., 2018a). Similar to SEQ, OPT captures the same chilling effect (Eq. (8)) as Eq. (3). Different from Eq. (4) in SEQ, the forcing is characterized using a sigmoid function (Eq. (9)) instead. In addition, the model also includes a new metric (Eq. (11)), the effectiveness of accumulated forcing that is constrained by both daylength  $DL(t)$  and chilling effects  $R_c(t)$ . Finally, LUD occurs on the date  $t_1$  when the realized forcing for photosynthetic carbon benefit (i.e.,  $S_f(t)$  in Eq. (12)) outweighs the potential negative impact associated with the frost damage risk (i.e.,  $a^* \exp(b^* S_c(t))$  in Eq. (12)).

$$R_c(t) = \begin{cases} \frac{T_t - T_{\min}}{T_{\text{opt}} - T_{\min}}, & T_{\min} \leq T_t < T_{\text{opt}} \\ \frac{T_t - T_{\text{opt}}}{T_{\max} - T_{\text{opt}}}, & T_{\text{opt}} \leq T_t < T_{\max} \\ 0, & \text{if } T_t < T_{\min} \text{ or } T_t > T_{\max} \end{cases} \quad (8)$$

$$R_f(t) = \begin{cases} 0, & T_t \leq T_{\text{base}} \\ \frac{28.4}{1 + \exp(3.4 - 0.185^* T_t)}, & T_t > T_{\text{base}} \end{cases} \quad (9)$$

$$S_c(t) = \sum_{t_0}^{t_1} R_c(t) \quad (10)$$

$$R_p(t) = \frac{DL(t)}{12} \times e^{c \times R_c(t)} \quad (11)$$

$$S_f(t) = \sum_{t_0}^{t_1} R_f(t) \times R_p, \text{ when } S_f(t) \geq a^* \exp(b^* S_c(t)) \text{ where } b < 0 \quad (12)$$

Where:  $R_c(t)$ ,  $R_f(t)$ , and  $R_p(t)$  indicate the states of chilling, forcing, and realized forcing effect on date  $t$ , and  $S_c(t)$  and  $S_f(t)$  indicate the accumulated chilling and forcing since  $t_0$  (set as January 1<sup>st</sup> of each year) to  $t_1$ ;  $T_{\text{base}}$  ( $= 5^\circ\text{C}$ ),  $T_{\min}$  ( $= -5^\circ\text{C}$ ),  $T_{\text{opt}}$  ( $= 10^\circ\text{C}$ ), and  $T_{\max}$  ( $= 25^\circ\text{C}$ ) are set as the same empirical constants as SEQ, following (Wang et al., 2020b); The model has three parameters to be fitted, i.e.,  $a$ ,  $b$ , and  $c$ .

### 2.3.2. Model calibration and validation

In this study, we trained and evaluated each of the three prognostic models (Section 2.3.1) using a 5-fold cross validation method (Yao et al., 2018) on a site-by-site basis, with satellite-derived LUD (Section 2.2.2) and environmental variables (Section 2.2.3) as inputs. Each site had a data record spanning approximately 20 years from 2001 to 2019. Since the three models had different number of parameters, a commonly used

approach for model selection is Akaike information criterion (AIC), the principle of which is to select the best-fit model that explains the greatest amount of variation using the fewest possible independent variables (Bozdogan, 1987). However, as (Stone, 1977) showed, minimizing the AIC is asymptotically equivalent to leave-one-out cross-validation. Thus, we used the 5-fold cross validation for cross-model comparisons, and recorded the corresponding  $R^2$  and RMSE as the model evaluation metrics.

The 5-fold cross validation method used in this study involved three steps. First, we randomly divided the full dataset into calibration and independent validation subsets using a 5-fold cross-validation with 20 repetitions. Second, for each repetition, we trained and evaluated the model for each of the three prognostic models. Third, we averaged the modelled LUD for each target site-year across all repetitions ( $n = 20$ ) to obtain an ensemble predicted value.

### 2.3.3. Assessing model residuals with other environmental variables

To explore whether other environmental variables that are not yet represented by current prognostic models also regulate spring phenology variability, we first calculated the model residuals (i.e., satellite-derived LUD minus modelled LUD) and then explored their relationships with preseason precipitation ( $P_{\text{pre}}$ ), preseason soil moisture ( $SM_{\text{pre}}$ ), and preseason shortwave radiation ( $SR_{\text{pre}}$ ). Notably, for each environmental variable, the preseason was simply defined as the period with the highest correlation coefficient between the environmental variable and LUD from 2001 to 2019 (Gao et al., 2019). The length of the preseason in months ranged from 1 to  $n$  and was defined as the time duration from LUD to its preceding  $i^{\text{th}}$  month, subject to  $0 < \text{LUD-}i \times 30 \text{ days} < \text{LUD}$  and  $0 < \text{LUD-}n \times 30 \text{ days} < 30$ . Afterwards, we used the partial correlation analysis (Piao et al., 2022) to explore how much the model residuals depended on each of the three variables while controlling for the effects of the other two variables.

### 2.3.4. Revised phenology models and model evaluation

After identifying the most important environmental variable(s) responsible for the model residuals (as described in Section 2.3.3), we next explored how to integrate these missing environmental cues with current prognostic models to improve the model performance of spring phenology. Specifically, our subsequent analysis demonstrated that  $SR_{\text{pre}}$  displayed the strongest and most significant partial correlation with the model residuals. We hypothesized that this is likely because solar radiation is a more effective variable than daylength  $DL(t)$  in indicating the potential photosynthetic carbon gain around leaf onset (Badeck et al., 2004; Yang et al., 2022). Consequently, we revised  $R_f(t)$  and/or  $R_p(t)$  in the original models of SEQ (i.e., Eq. (4)) and OPT (i.e., Eq. (11)) by replacing the relevant  $DL(t)$  with  $SR(t)$  as shown in Eq. (13).

$$SR(t) = k \times (SR_t - SR_0) \quad (13)$$

Where:  $k$  is (site-specific) scalar constant value;  $SR_t$  and  $SR_0$  respectively indicate the shortwave radiation on date  $t$  and the constant threshold (applicable to all sites) of shortwave radiation to remove the magnitude difference that exerts a role in constraining  $S_f(t)$ .

With the revised models as described above, we evaluated their effectiveness and the soundness of the underlying hypothesis in two ways. First, we explored whether the revised models would generate significant improvements in their model performance (e.g., RMSE), especially relative to the default models that relied on daylength  $DL(t)$  as a predictor. Second, to ensure that the model performance improvement is not at the cost of increasing model residuals to other variables (in addition to daylength), we calculated the Pearson partial correlation to measure the degree of association between the model residual and all other environmental variables.

### 3. Results

#### 3.1. Evaluating the prognostic model performance for modelling spring phenology

Our results show that all three prognostic models (i.e., GDD, SEQ, and OPT) reasonably characterized the temporal variation in spring phenology of each site over approximately 20 years (Fig. 2(a)&(e)). The OPT model had the highest performance ( $R^2 = 0.53 \pm 0.24$  [1std]; RMSE =  $8.04 \pm 5.05$  [1std] days across all sites), followed by SEQ ( $R^2 = 0.27 \pm 0.23$ , RMSE =  $10.57 \pm 7.77$  days) and GDD ( $R^2 = 0.29 \pm 0.22$ , RMSE  $10.84 \pm 8.42$  days). Additionally, we observed significant variation in modelling accuracy across all study sites, with RMSE ranging from 3.67 (10th percentile) to 14.90 (90th percentile) days for the OPT model, 4.29 to 18.23 days for SEQ, and 3.91 to 20.99 days for GDD.

OPT also had the highest performance among all three models in modelling spring phenology, consistently across the three PFTs of DBF, GRA, and MXF (Fig. 2). The models performed the best in DBF, particularly in terms of RMSE ( $6.08 \pm 3.15$  days for OPT;  $7.46 \pm 3.62$  days for SEQ;  $7.34 \pm 3.95$  days for GDD), followed by MXF ( $7.66 \pm 2.58$  days for OPT;  $8.45 \pm 3.16$  days for SEQ;  $8.47 \pm 3.60$  days for GDD) and GRA ( $11.24 \pm 6.29$  days for OPT;  $16.03 \pm 10.19$  days for SEQ;  $16.99 \pm 10.81$  days for GDD) (see Fig. 2).

To further evaluate whether the observed relative order of these prognostic models is statistically significant, we calculated the accuracy difference between each pair of models for each site and performed a histogram analysis to assess the distribution of these differences across all sites (Fig. 3(a)&(e)). Our results indicate that over 77% of all sites showed an increase in  $R^2$  and a decrease in RMSE when using the OPT model relative to the SEQ model, with a mean increase of  $R^2 = 0.25$  and a mean reduction of RMSE = 2.52 days across all sites. The t-test results (Table S1) were consistent with the pair analysis, indicating that OPT significantly outperformed SEQ in modelling spring phenology. Moreover, >51% of all sites exhibited higher  $R^2$  and lower RMSE in SEQ compared to GDD, and the t-test results comparing these two models were significant (Table S1). However, the difference in performance between SEQ and GDD was marginal (Fig. 3).

At the PFT level, the DBF and GRA sites demonstrated much better performance in the OPT model relative to the SEQ model, while the performance difference between the two models was smaller in MXF (Fig. 3 and Table S1). Additionally, the SEQ model showed comparable performance to the GDD model in DBF and GRA, but it performed much better in MXF (Fig. 3 and Table S1).

#### 3.2. Exploring the model residual and its association with key environmental variables

Across all sites, our findings demonstrate that the model residuals consistently exhibited the strongest partial correlations with  $SR_{pre}$  (i.e., the across-all-sites mean value of correlation coefficient  $r > 0.5$ ), and moderate-to-little partial correlations with  $P_{pre}$  and  $SM_{pre}$  (i.e., the absolute value of mean  $r < 0.3$ ) (Fig. 4 and Table S3). These observations hold true regardless of the model the residuals are derived from. Notably, the partial correlation of  $SR_{pre}$  was significantly higher in GDD ( $r = 0.79 \pm 0.21$ ) and SEQ ( $r = 0.80 \pm 0.19$ ) compared to OPT ( $r = 0.60 \pm 0.25$ ) (Fig. 4a).

At the PFT level, the model residuals also showed the strongest partial correlation with  $SR_{pre}$  and moderate-to-little partial correlations with the other two environmental variables. Meanwhile, there were minor variations in the partial correlations of model residuals with environmental variables across different PFTs. Since the results across the three prognostic models were similar (Fig. 4), we used OPT as an example for illustration. As seen in Fig. 4,  $SR_{pre}$  exhibited the highest partial correlation with model residuals among all three environmental variables. The partial correlation coefficient of  $SR_{pre}$  was  $0.60 \pm 0.25$  for all sites,  $0.63 \pm 0.20$  for DBF,  $0.55 \pm 0.31$  for GRA, and  $0.60 \pm 0.29$  for MXF. The partial correlations of model residuals with  $P_{pre}$  had much higher variations across different PFTs, with  $P_{pre}$  exhibiting the partial correlation of  $-0.04 \pm 0.29$  for all sites,  $-0.06 \pm 0.26$  for DBF,  $-0.03 \pm 0.34$  for GRA, and  $0.04 \pm 0.27$  for MXF. As for  $SM_{pre}$ , there was very little fluctuation in the partial correlation across PFTs, with  $SM_{pre}$  holding a partial correlation of  $-0.06 \pm 0.28$  for all sites,  $-0.07 \pm 0.27$  for DBF,  $-0.09 \pm 0.31$  for GRA, and  $-0.05 \pm 0.30$  for MXF.

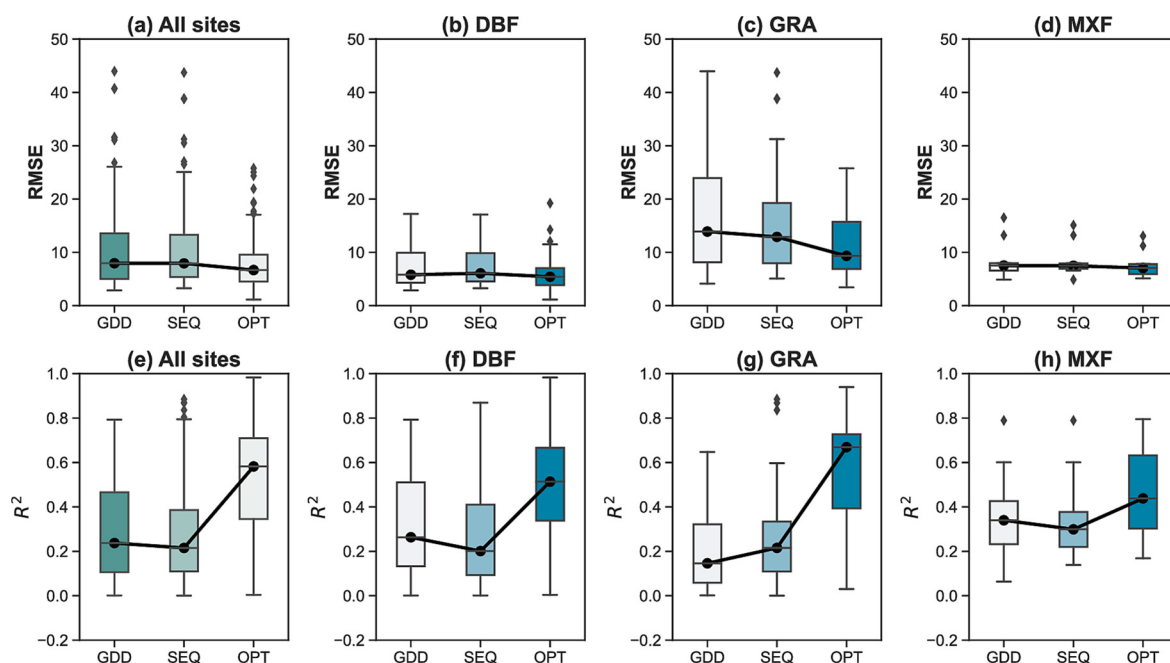


**Fig. 2.** The performance of the three prognostic models in modelling spring phenology, using the two accuracy metrics of RMSE (top panels) and  $R^2$  (bottom panels). Model performance was assessed at both across-all-sites ( $n = 108$  sites; a, e) and at the PFT levels of deciduous broadleaf (DBF;  $n = 60$  sites; b, f), grassland (GRA;  $n = 38$  sites; c, g), and mixed forest (MXF;  $n = 10$  sites; d, h).

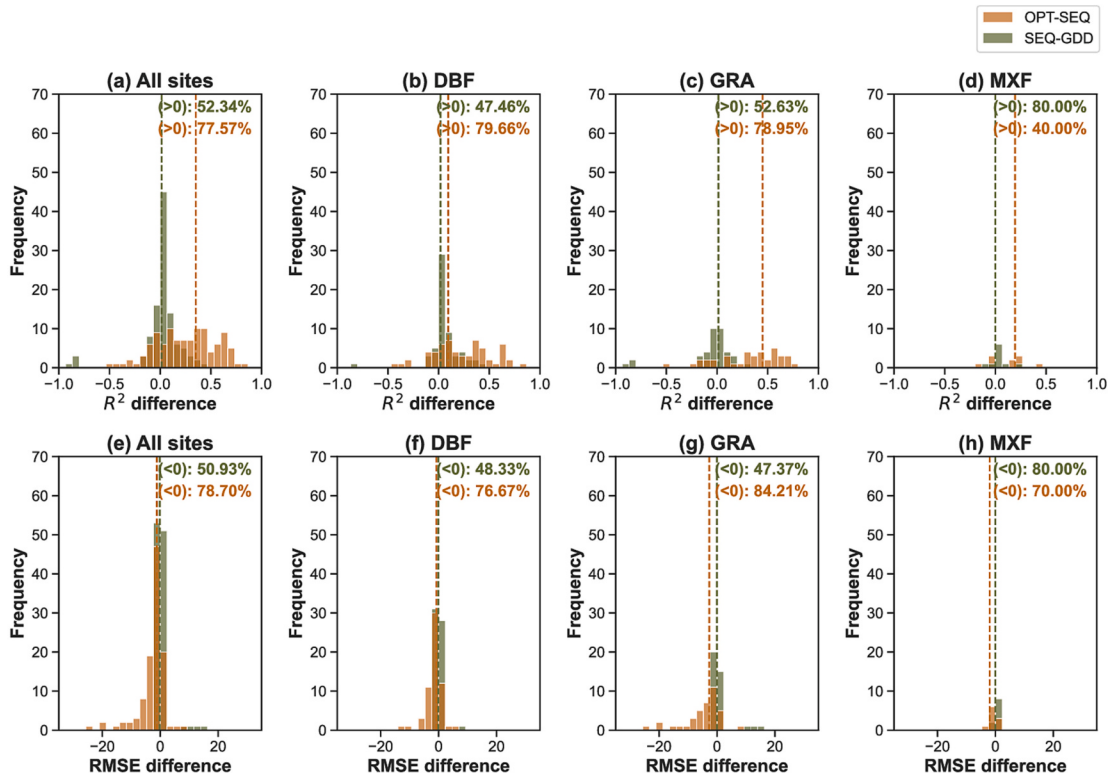


**Fig. 3.** Histogram analysis on the paired model performance difference, using the two accuracy metrics of  $R^2$  (top panels) and RMSE (bottom panels). Model performance difference was assessed at both across-all-sites (a, e) and at the PFT levels of deciduous broadleaf (DBF; b, f), grassland (GRA; c, g), and mixed forest (MXF; d, h). Notably, OPT-GDD indicates the site specific model metric of OPT minus its corresponding GDD model metric; SEQ-GDD indicates the site specific model metric of SEQ minus its corresponding GDD model metric.

### 3.3. Exploring the performance of revised models and their model residual associations with key environmental variables

Our results in Fig. 5 showed that the revised models that included  $SR_{pre}$  significantly improved the performance in modelling spring phenology compared to the default models (Fig. 6(a)&(e) and Table S2). Over 70% of all sites demonstrated an improvement in performance, with the improvement being consistent for both SEQ and OPT models. Across all sites, there was an average increase of 0.29 in SEQ and 0.09 in OPT for  $R^2$ , and an average reduction of 2.82 days in SEQ and 1.41 days in OPT for RMSE (Fig. 5(a)&(e)). Across different PFTs, model accuracy displayed the highest improvement in MXF (SEQ:  $R^2$  increased by 0.28 and RMSE reduction by 1.94 days; OPT:  $R^2$  increased by 0.24 and RMSE reduction by 2.78 days), followed by GRA (SEQ:  $R^2$  increased by 0.35 and RMSE reduction by 2.30 days; OPT:  $R^2$  increased by 0.22 and RMSE reduction by 2.36 days), and the least in DBF (SEQ:  $R^2$  increased by 0.25 and RMSE reduction by 1.68 days; OPT:  $R^2$  increased by 0.06 and RMSE reduction by 0.58 days) (Fig. 5(b)-(d), (f)-(h)). Furthermore, we found that the revised OPT model (OPT\_rev) performed the best with an all-site-mean  $R^2 = 0.62 \pm 0.26$  and RMSE =  $6.63 \pm 4.83$  days, followed by the revised SEQ model (SEQ\_rev) with an all-site-mean  $R^2 = 0.56 \pm 0.24$  and RMSE =  $7.75 \pm 5.88$  days. The default OPT model had an  $R^2$  of  $0.53 \pm 0.24$  and RMSE of  $8.04 \pm 5.05$  days, followed by the default SEQ with an  $R^2$  of  $0.27 \pm 0.23$  and RMSE of  $10.57 \pm 7.77$  days, and GDD with an  $R^2$  of  $0.29 \pm 0.22$  and RMSE =  $10.84 \pm 8.42$  days. We also found that replacing daylength with solar radiation significantly improved model performance by reducing the RMSE for all PFTs. The improvement of RMSE from the 25th percentile (Q1) to the 75th percentile (Q3) changed from 4.55 to 9.85 days in SEQ for DBF to 4.33–6.99 days in SEQ\_rev, for GRA from 7.95 to 19.24 days to 6.23–14.45 days, and for MXF from 6.92 to 7.94 days to 4.97–7.28 days. Similarly, the improvement of RMSE in OPT from Q1 to Q3 changed from 3.85 to 7.03

days in OPT to 3.66–6.20 days in OPT\_rev for DBF, for GRA from 6.88 to 15.71 days to 4.81–10.49 days, and for MXF from 5.91 to 7.78 days to 3.11–6.46 days. These changes provided strong evidence for the significant improvement in model performance with the inclusion of SR.

The revised models significantly reduced the partial dependency of model residuals on  $SR_{pre}$ , with little-to-moderate change in other environmental variables (Fig. 7(b)-(d), Fig. S2 and Table S4–5). These observations were consistent despite pooling all the site data together or analyzing the results at the PFT level, and were also consistent across the two models of SEQ and OPT (Fig. 7). Since the results of the two revised models were similar, we used OPT\_rev as an example for illustration. From Fig. 7a, the average partial correlation of model residuals with  $SR_{pre}$  significantly reduced from  $0.60 \pm 0.25$  in OPT to  $0.50 \pm 0.28$  in OPT\_rev across all sites (with the all-site-mean partial correlation reduced from  $0.80 \pm 0.19$  in SEQ to  $0.58 \pm 0.25$  in SEQ\_rev), with little-to-moderate change in the average partial correlation for the other three environmental variables (i.e.,  $r$  changed from  $-0.04$  to  $0.00$  for  $P_{pre}$ , from  $-0.05$  to  $0.02$  for  $SM_{pre}$ ; from  $0.16$  in OPT to  $0.20$  in OPT\_rev for  $DL_{pre}$ ; Fig. 7). At the PFT level,  $SR_{pre}$  remained the environmental variable showing the highest partial correlation with model residuals, consistently across both SEQ\_rev and OPT\_rev. Meanwhile, moderate variations in partial correlation changes (between SEQ and SEQ\_rev and between OPT and OPT\_rev) remained among all three PFTs (Fig. 7, Fig. S2, and Table S4–5), and for most partial correlation changes, the revised model displayed a significant reduction or at least no significant increase in the model residual partial dependency on any of the four environmental variables. Finally, when evaluating the partial relationship between  $SR_{pre}$  and  $DL_{pre}$  (conditioned by removing their independent contribution to LUD) at both the across and within sites levels, we found that the across-all-sites partial correlation between  $SR_{pre}$  and  $DL_{pre}$  was 0.49, while most sites ( $n = 105$  among all 108 sites) had a within-site partial correlation coefficient lower than 0.49 (Fig. 7e),

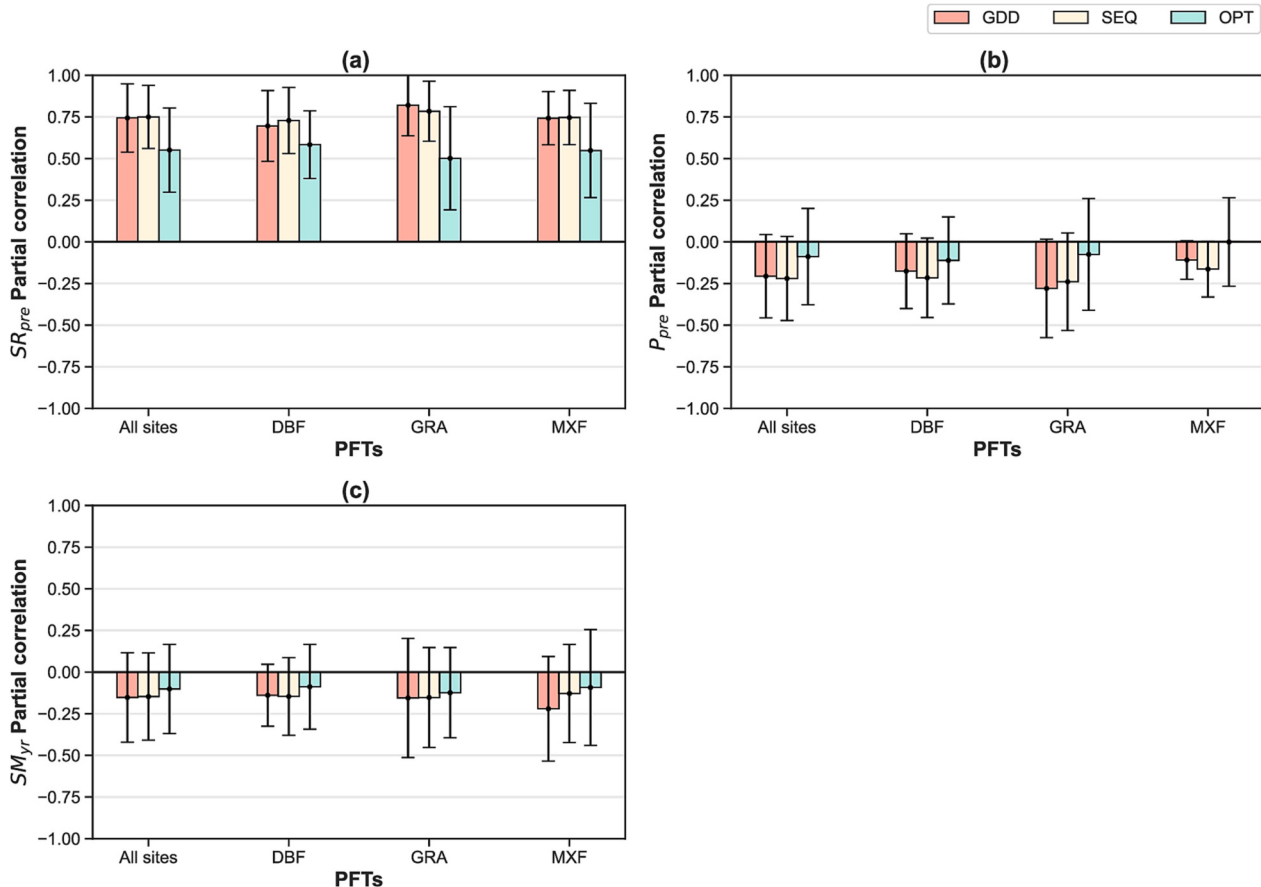


**Fig. 4.** The partial dependency of model residuals with three environmental variables of preseason solar radiation ( $SR_{pre}$ ; a), preseason precipitation ( $P_{pre}$ ; b), and preseason soil moisture ( $SM_{pre}$ ; c). Notably, the model residuals were assessed using MODIS-derived LUD minus model-predicted LUD, including all the three models of GDD (orange), SEQ (light yellow), and OPT (light green); the partial correlation analysis was conducted on a site basis across an approximately 20 years duration and the results were respectively displayed at all-sites and each PFT levels. (For interpretation of the references to colour in this figure legend, the reader is referred to the web version of this article.)

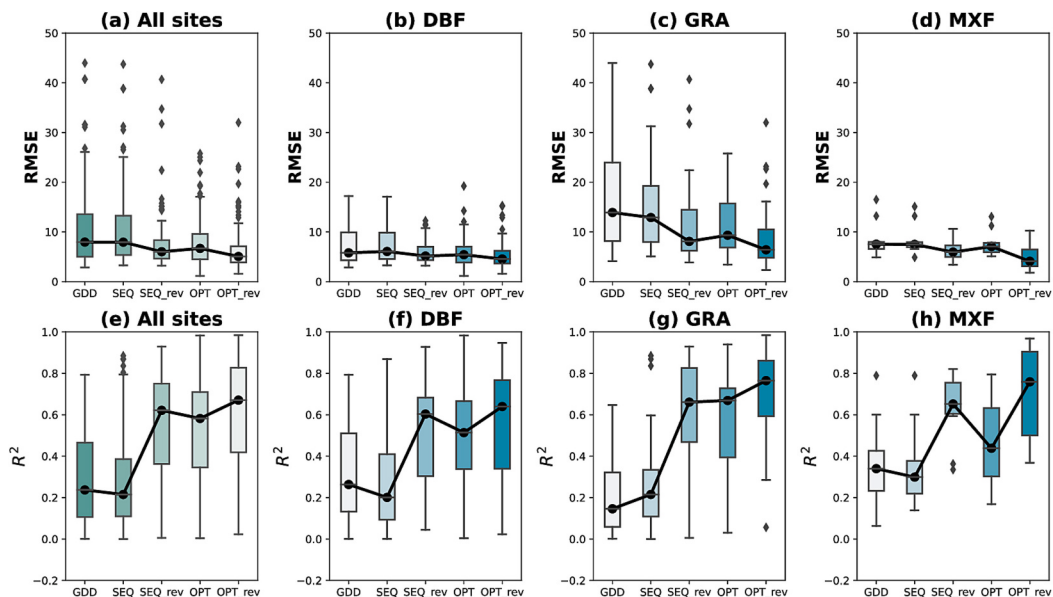


**Fig. 5.** The performance of the three prognostic models and two revised models (SEQ\_rev and OPT\_rev) in modelling spring phenology, using the two accuracy metrics of RMSE (top panels) and  $R^2$  (bottom panels). Model performance was assessed at both across-all-sites and at the PFT levels of deciduous broadleaf (DBF; b, f), grassland (GRA; c, g), and mixed forest (MXF; d, h).

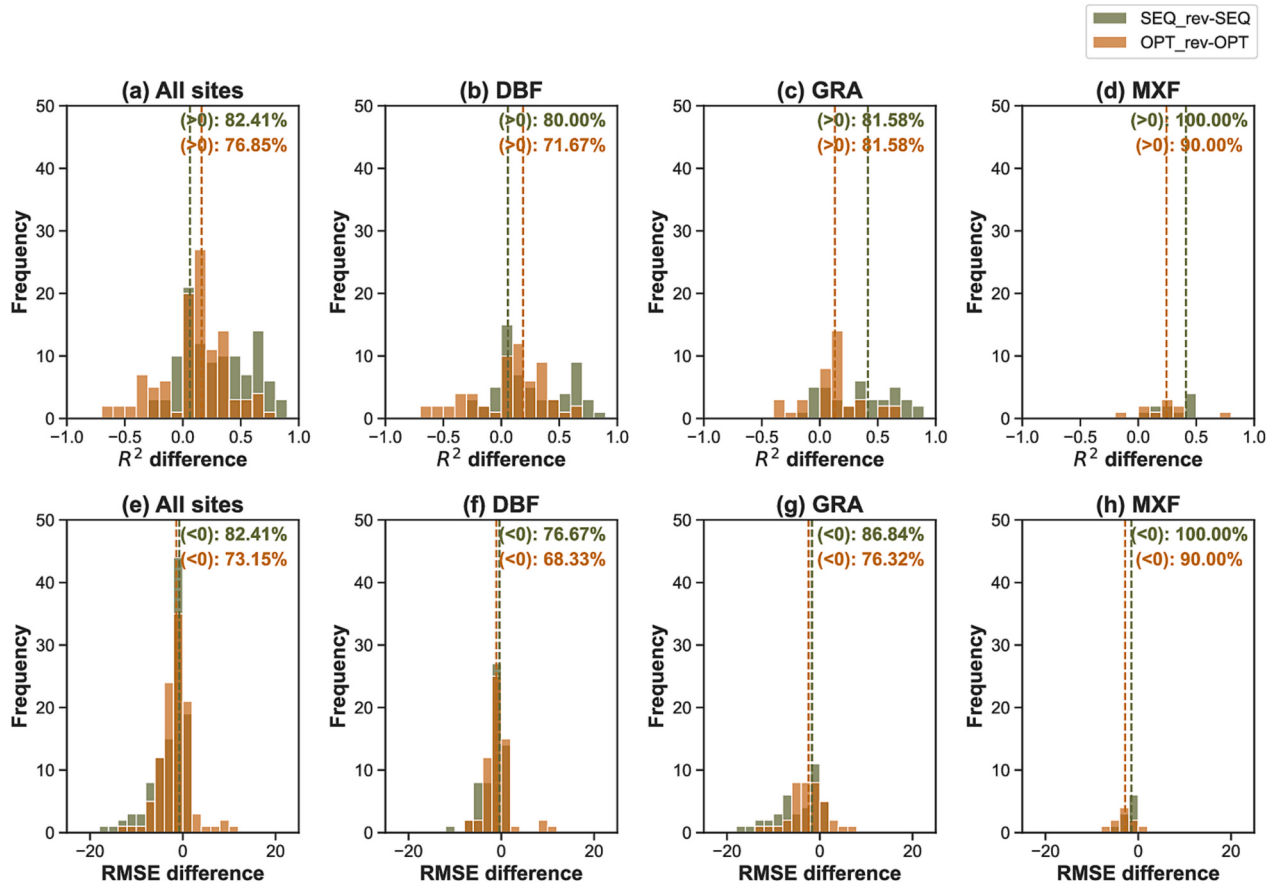


**Fig. 6.** Histogram analysis on the paired model performance difference, using the two accuracy metrics of  $R^2$  (top panels) and RMSE (bottom panels). Model performance difference was assessed at both across-all-sites (a, e) and at the PFT levels of deciduous broadleaf (DBF; b, f), grassland (GRA; c, g), and mixed forest (MXF; d, h). Notably, SEQ\_rev-SEQ indicates the site specific model metric of SEQ\_rev minus its corresponding SEQ model metric; OPT\_rev-OPT indicates the site specific model metric of OPT\_rev minus its corresponding OPT model metric.

demonstrating that the  $SR_{pre}$ - $DL_{pre}$  relationship was more decoupled within each study site over the near 20-year time duration.

#### 4. Discussion

##### 4.1. The underappreciated importance of solar radiation in constraining spring phenology and potential underlying mechanisms

Our study demonstrates that large model residuals associated with preseason solar radiation ( $SR_{pre}$ ) persist consistently across all three models (GDD, SEQ and OPT; Fig. 4a), implying that an important mechanism related with  $SR_{pre}$  is missing in the current models. Solar radiation not only reflects daylength changes (Fig. 7e), but also affects complex early-season weather conditions (e.g., clouds and snow) that importantly influence plant ecosystem phenology. As such, we hypothesized that  $SR$  could be a more effective variable than daylength for driving spring phenology. Our results support this hypothesis by showing that the revised models (with  $SR$  and  $T_a$  as inputs) perform better than the default models with  $DL$  and  $T_a$  as inputs (Figs. 5&6) without significantly affecting the partial dependency of model residuals on other environmental variables, including  $DL_{pre}$  that was replaced (Fig. 7). This suggests that replacing  $DL$  with  $SR$  represents an effective way to improve the prognostic models for modelling spring phenology in these temperate ecosystems.

There are two potential reasons underlying the above findings. First, solar radiation tends to be a more suitable variable than daylength in this regard. As illustrated earlier, spring phenology is connected to three critical phenophases: endodormancy, ecodormancy, and active growth

period. Despite several studies suggesting that photoperiod (or daylength) can be an important environmental trigger for ecodormancy and the active growth period (Caffarra et al., 2011; Flynn and Wolkovich, 2018; Ma et al., 2021), daylength is mainly determined by site latitude and does not vary from year to year. Thus, if daylength is used in the prognostic models for inferring spring phenology variability within a site over years, it would risk in under-emphasizing the role of other environmental variables, like temperature (to constrain not only endodormancy but also ecodormancy and the active growth period). Meanwhile, when interacting with other site properties (e.g., topography, long-lasting snow cover), solar radiation could create more complex microclimate variations (Hwang et al., 2011; Yun et al., 2018). For example, ambient light conditions, in addition to daylength, interact with temperature to prevent plants from leafing out prematurely and suffering from frost damage (Meng et al., 2021b). The better model performance with  $SR$  than  $DL$  thus implies either 1)  $SR$  is a better proximate environmental cue for spring phenology or 2) the  $SR_{pre}$  is more dynamics than daylength on an interannual time-scale, and can be a more important control on spring phenology than daylength.

The second reason is related with the subject of spring phenology control subject to fundamental eco-evolutionary optimality constraints (Fu et al., 2019), as shortwave radiation is a more direct variable than daylength in determining plant photosynthesis rates (Herrmann et al., 2020) and the start of the photosynthetically active season (Zhang et al., 2020b). As shown in Figs. 2 and 5, OPT performs the best among all the three prognostic models, suggesting that the theory underlying the OPT model would operate the best in mediating spring phenology variability. The fundamental theory of OPT lies in the hypothesis of spring

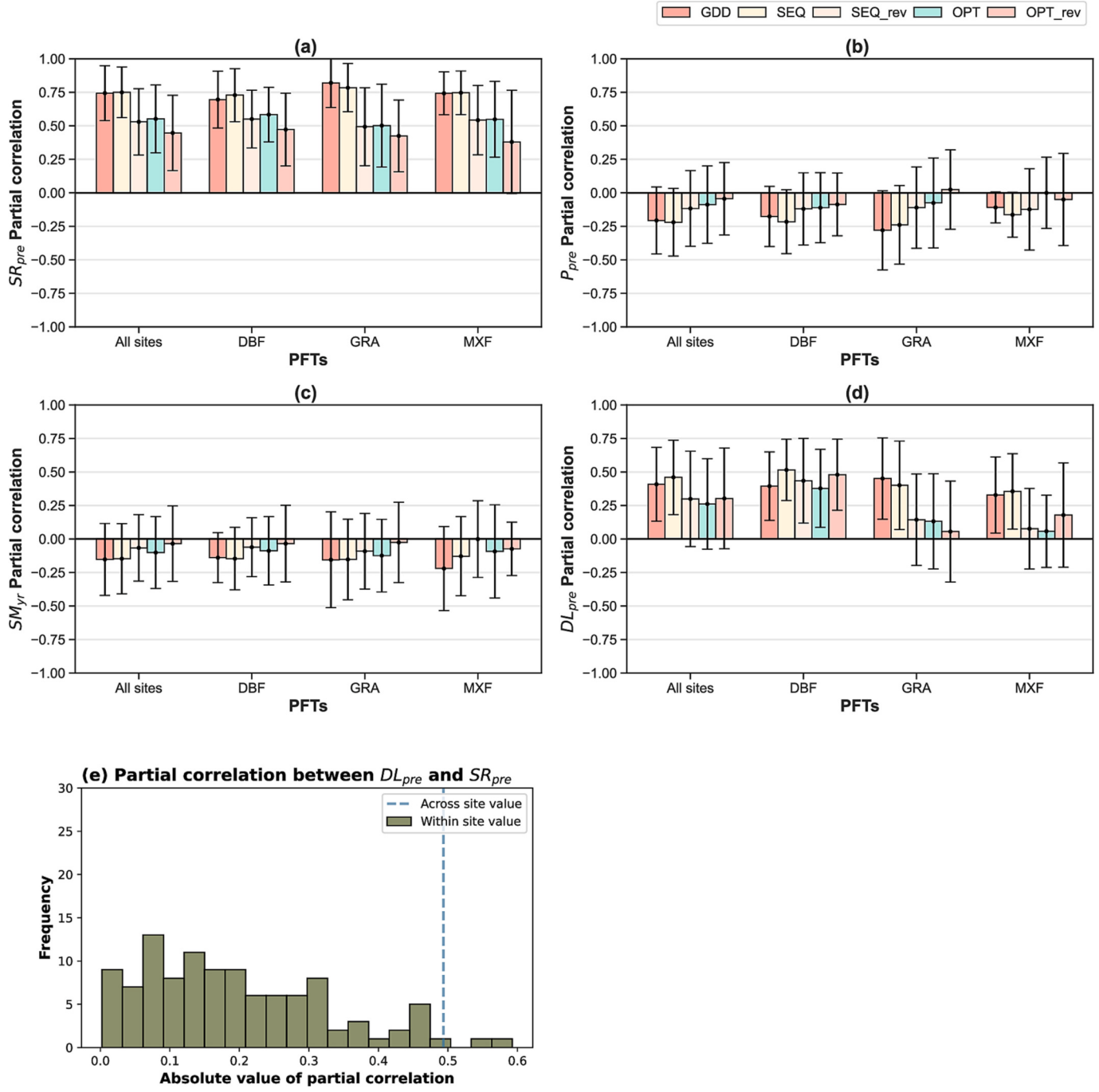


**Fig. 7.** The partial dependency of model residuals with four environmental variables of preseason solar radiation ( $SR_{pre}$ ; a), preseason precipitation ( $P_{pre}$ ; b), preseason soil moisture ( $SM_{pre}$ ; c) and preseason daylength ( $DL_{pre}$ ; d). The partial correlation between  $DL_{pre}$  and  $SR_{pre}$  conditioned by removing their independent contribution to LUD at the two levels of across-all-sites and within-each-site was also displayed (e). Notably, in panels a-d, the model residuals were assessed using MODIS-derived LUD minus model-predicted LUD, including all the three models of GDD, SEQ, and OPT and two revised models of SEQ\_rev and OPT\_rev; the partial correlation analysis was conducted on a site basis across an approximately 20 years duration and the results were respectively displayed at all-sites and each PFT levels; in panel e, the dash blue line indicated the across-all-site result while the histogram summarized the within-site statistics across all 108 sites.

phenology as an optimal strategy for plants to minimize frost damage risk while maximizing photosynthetic carbon gain (Bennie et al., 2010; Estrella et al., 2017; Fu et al., 2019; Zohner et al., 2020b). In this trade-off between frost damage risk and photosynthetic carbon gain, photosynthetic carbon gain is more related with  $SR$  than  $DL$  due to its direct constraint on plant photosynthesis rates (Descals et al., 2022; Durand et al., 2021; Farquhar et al., 1980; Sun et al., 2019).

Our finding that  $SR$  is a better variable than  $DL$  to constrain spring phenology has not been reported previously. This is largely because

most of previous research was conducted at the PFT level or beyond, in which the latitude gradient dominates the spatial variation in both  $DL_{pre}$  and  $SR_{pre}$ , and it is not surprising to observe a tight correlation between them across large spatial extents (Fu et al., 2019; Meng et al., 2021b; Vitasse et al., 2011; Wang et al., 2021). However, in our study, we demonstrated for the first time that there was a decoupled relationship between  $DL_{pre}$  and  $SR_{pre}$  within a site across the decadal time duration (Fig. 7e). Such a contrast of the  $DL_{pre}$ - $SR_{pre}$  relationship between within-site and across-site analyses further raises a concern that the

conventional PFT level (or beyond) prognostic models might risk in mixing the temporal and spatial variability of spring phenology's response to climate change in temperate regions, as the fundamental mechanism related with  $SR_{pre}$  in mediating within-site temporal phenology variability is not well captured. Meanwhile, it is unrealistic in the real world to calibrate the spring phenology model on a site level as conducted in this study (which might risk in overfitting and can be sensitive to phenological outliers). Thus, future attempts to assess a more appropriate mid-stage (between site and PFT levels) for calibrating and using these prognostic models would be greatly needed, but this is beyond the scope of this paper.

#### 4.2. The good capability of current prognostic models for characterizing the spring phenology variability over time at the ecosystem level

Although prognostic models for spring phenology modelling have been proposed and evaluated on the organism/species level (Caffarra et al., 2011; Dai et al., 2019; Meng et al., 2021b; Way and Montgomery, 2015), and some have also been evaluated on the ecosystem level (Fisher et al., 2007; Migliavacca et al., 2011; Post et al., 2022; Wang et al., 2020a), a comprehensive assessment of ecosystem-level phenology mechanisms and modelling across large spatial coverage and over a decadal time duration remains lacking. In this study, we leveraged the MODIS satellite-derived spring phenology metric and evaluated these models on a site-by-site basis over nearly 20 years across 108 temperate sites in Northern and Eastern United States. Our results demonstrate that these models reasonably characterized the temporal variability in ecosystem-level spring phenology (Fig. 2), demonstrating the good capability of extending the current prognostic modelling framework from the organisms/species level to the ecosystem level.

Among all three models examined in this study, we found that OPT performed the best, followed by SEQ and GDD (Figs. 2 & 3; Table S1). This finding is consistent with recent studies that demonstrate that OPT is more accurate, and potentially more mechanistic, for modelling spring phenology in temperate ecosystems (Kim et al., 2022; Meng, 2021; Meng et al., 2021a; Meng et al., 2021b). Because the OPT model considers the parallel relationship between endodormancy and ecodormancy periods, which differs from SEQ (which uses the sequential relationship) and GDD (which relies only on the single accumulated forcing threshold criteria), our finding suggests that OPT better describes the dependent relationship between how plants endure an unfavourable cold environment (or endodormancy, captured by the chilling effect) and how the ambient environment triggers the transition from the ecodormancy period to the active growth period (captured by the interactive effect between forcing and photoperiod (Fig. 2) or solar radiation (Fig. 5)).

Furthermore, consistent with previous studies (Fu et al., 2021; Marchand et al., 2020; Moon et al., 2021b), we observed large variations in model performance across different PFTs, with the models performing best in DBF, followed by MXF and GRA (Fig. 2). This is likely because DBF displays higher sensitivity to the heat requirement for release from the dormancy period than other PFTs, and thus is better characterized by these models (Descals et al., 2022; Richardson et al., 2013). Conversely, for MXF and GRA, environmental variables other than temperature, such as precipitation (Yun et al., 2018) or topography (Hwang et al., 2011), might also constrain their spring phenology variability (Cleland et al., 2006; Donnelly et al., 2017; Felton et al., 2020), resulting in relatively poorer model performance. Additionally, the more complex plant compositions in MXF and GRA (especially at a pixel resolution of 500 m MODIS) than in DBF, and the differential phenological sensitivity response to ambient environment fluctuations among these different compositions (Donnelly et al., 2017; Richardson et al., 2018b), could also worsen the model performance if the effect of complex compositions is not explicitly considered. Future research efforts with higher-resolution LSP data records (e.g., Moon et al., 2022; Zhao et al., 2022) and characterizations of forest composition (e.g., Zanaga et al., 2022) could be essential to improve the elucidation of the underlying spring

phenology mechanisms across different PFTs.

Finally, we observed consistent model performance improvements across all three PFTs (Fig. 5), providing compelling evidence that integrating the process of solar radiation is necessary for improving spring phenology modelling for all the studied PFTs. Further analysis also shows that these model performance improvements are significant relative to their original performance (Fig. 6) and have a magnitude of improvement significantly higher than the inherent model uncertainties associated with model constants (Fig. S3), suggesting that these model improvements are not marginal. Additionally, all sets of model parameters (Table S6–10) generated by this study and the potential extension of this research to broader scales using long-time series satellite LSP data could provide necessary parameterizations to improve the use of these prognostic models for simulating spring phenology response to longer-term climate change and variability.

#### 4.3. Uncertainties and future directions

There are at least four sources of uncertainty in the data analysis that may affect our findings. First, to evaluate the prognostic models' performance, we used the satellite-derived spring phenology metric generated by Friedl et al. (2019) as the benchmark. Although this phenology product has been rigorously evaluated (Friedl et al., 2019) and demonstrated good accuracy when comparing with local phenocam observations (Fig. S1), there remain other sources of uncertainty in the retrieved spring phenology metric, such as coarse spatial resolutions (i.e., mixed pixel effect associated with different plant species compositions or PFTs), noise caused by residual atmospheric effects of clouds, hazes, and aerosols, and snow contaminations, especially at high latitudes (Ma et al., 2022). Meanwhile, the mixture of multiple individuals in the ecosystem also brings uncertainty, as biases have been found between the algorithms-derived leaf unfolding date and actual phenostages such as budburst or leafout from finer scale observational dataset such as PEP725, US-NPN, and other in-situ data (Moon et al., 2021a; Richardson et al., 2018c). To address this, future improvements of phenological retrieval algorithms and more rigorous data quality control procedures would still be needed (Ma et al., 2022), especially when extending our current research conducted on hundreds of sites in the United States to an even larger area around the world using satellite remote sensing. Second, we used approximately 20-year phenological records from the MODIS satellite to examine the capability of existing prognostic models. However, the range of near 20 years phenological variability varied considerably from site to site. Since a higher range of phenological variability across the decadal timescale often means a higher confidence in calibrating the prognostic models and subsequent mechanistic explorations, sites with smaller ranges may pose a risk in calibrating and evaluating the prognostic models. Future phenology products with longer temporal duration and improved product accuracy remain greatly needed to evaluate the application of these prognostic models. Third, there remains a considerable residual partial dependency of the model on  $SR_{pre}$  (Fig. 7), suggesting that the impact of  $SR_{pre}$  on spring phenology (e.g., via photosynthetic carbon gain) could be more complex than the way it is currently modelled (i.e., using a linear model; Eqns. 4 and 11).  $SR$  can directly and indirectly affect plant photosynthesis rates: 1) the direct effect is primarily through the light-photosynthesis relationship, whereby plant photosynthesis rate increases nearly linearly with  $SR$  in the early season with low light conditions (Jumrani and Bhatia, 2020); 2) the indirect effect is because the early season temperature rise associated with the  $SR$  increase could also affect plant photosynthesis rate by mediating the maximum carboxylation rate (or  $V_{cmax}$ ) following the Arrhenius equation in an exponential way (Medlyn et al., 2002). Therefore, the representation of solar radiation constraints on plant photosynthetic carbon gain in current prognostic models is imprecise and could be improved. Fundamental theories and models in the plant ecophysiology field, such as the Farquhar-type photosynthesis model (Farquhar et al., 1980), could be used to

improve the future prognostic model development (Xu et al., 2017). Meanwhile, recent advancements in observational technology, such as the increasing availability of ground and satellite-based solar radiation monitoring and the increasing maturity of process model-data fusion techniques, have made accurate and high-temporal-resolution solar radiation data increasingly available at the regional (e.g., NSRDB, ESRA; Rigollier et al., 2000; Sengupta et al., 2018) and global (e.g., ERA5-Land; Muñoz-Sabater et al., 2021) scales. These data can facilitate the use of revised phenology models (including solar radiation as model input), as suggested in this study. Nevertheless, the incorporation of solar radiation data into models may introduce data uncertainty, and future studies are still needed to assess its potential impact on spring phenology modelling on a large scale. Fourth, although our sensitivity analysis (Fig. S3) suggests that our modelling results are not sensitive to the predefined model constants, such as  $T_{min}$ ,  $T_{max}$ , and  $T_{base}$ , we still recommend that these model constants should still be used with caution, especially when applying these prognostic models to more diverse terrestrial ecosystems.

Our work also identified at least two important directions for future phenology-related studies. First, in our study of temperate ecosystems in the United States, we found that SR is a key missing environmental variable that is under-represented in current prognostic models. This finding is generated because the spring phenology of these study sites is known to be limited by temperature (a process of which is well captured by current models), and thus we can focus on examining which of SR and DL is more related with plants' potential photosynthetic carbon gain—another process to constrain the start of spring phenology and subsequent active growth period. However, when moving beyond these temperate forest sites, other environmental variables, such as rainfall (Li et al., 2020; Ren and Peichl, 2021), soil moisture (Huang et al., 2019; Tao et al., 2020b), snow (Yun et al., 2018), and elevation (Vitasse et al., 2018), might also exert roles in constraining spring phenology. Therefore, a critical next step is to expand the analysis to an even larger area using remote sensing data to identify regions where spring phenology is constrained by temperature, water, or other factors, and investigate whether there is a generalizable modelling framework to advance spring phenology modelling across diverse terrestrial ecosystems. Second, since spring phenology has been shown to be tightly associated with many important ecosystem processes, such as spring carbon sequestration (Delpierre et al., 2016; Galvagno et al., 2013), land surface energy balance (Moon et al., 2021b), early growing season water use (Wu et al., 2022), and many others (Mäkiranta et al., 2018), our attempt to improve spring phenology modelling would inspire subsequent integration with more complex terrestrial biosphere models. This would allow us to examine how these improvements in spring phenology modelling might help better assess terrestrial ecosystems response to climate change.

## 5. Conclusion

In this study, we explored how well three prognostic models characterized the decadal spring phenology variability in the studied temperate ecosystems, among which OPT performed the best, followed by SEQ and GDD (Figs. 2–3). The model residuals of all three model showed a very high partial correlation with preseason shortwave radiation, suggesting shortwave radiation importantly regulated the spring phenology of temperate ecosystems, which had not been involved in current prognostic models (Fig. 4a). To improve the performance of current models, we replaced the daylength with shortwave radiation and found that the revised models performed significantly better, with an RMSE reduction by 22.08% (Figs. 5–6). Meanwhile, this improvement had little-to-no effect on the partial dependency of these model residuals on other environmental variables (Fig. 7a-d). Collectively, our study demonstrates that temperature coupling solar radiation effect is better tightly associated with the spring phenology biophysical process under natural scenarios, which provides insights to improve many other phenology-related ecosystem processes in terrestrial biospheres models

and further benefits the accurate predictions of temperate ecosystems' response to climate change.

## CRediT authorship contribution statement

**Yating Gu:** Conceptualization, Investigation, Methodology, Software, Formal analysis, Visualization, Data curation, Writing – original draft, Writing – review & editing. **Yingyi Zhao:** Conceptualization, Investigation, Writing – review & editing. **Zhengfei Guo:** Conceptualization, Investigation, Writing – review & editing. **Lin Meng:** Investigation, Writing – review & editing. **Kun Zhang:** Writing – review & editing. **Jing Wang:** Writing – review & editing. **Calvin K.F. Lee:** Writing – review & editing. **Jing Xie:** Writing – review & editing. **Yantian Wang:** Writing – review & editing. **Zhengbing Yan:** Writing – review & editing. **He Zhang:** Writing – review & editing. **Jin Wu:** Conceptualization, Supervision, Resources, Writing – original draft, Writing – review & editing, Funding acquisition.

## Declaration of Competing Interest

The authors declare that they have no known competing financial interests or personal relationships that could have appeared to influence the work reported in this paper.

## Data availability

Data will be made available on request.

## Acknowledgements

We would like to thank the editors and three reviewers for providing valuable suggestions and comments, which are greatly helpful in improving the quality of this work. This work was supported by National Natural Science Foundation of China (#31922090) and Hong Kong Research Grant Council General Research Fund (#17305321). J.Wu was supported by the HKU Seed Funding for Basic Research (202011159154), the HKU Seed Funding for Strategic Interdisciplinary Research Scheme, the Hung Ying Physical Science Research Fund 2021-22, and the Innovation and Technology Fund (funding support to State Key Laboratories in Hong Kong of Agrobiotechnology) of the HKSAR, China. L.M. was in part supported by the NASA FINESST Program "NNH19ZDA005K." J.Wang was in part supported by Shenzhen Science and Technology Program (Grant No. 20220816162849005) and the Division of Ecology and Biodiversity PDF research award. CKFL was in part supported by HKU seed fund for basic research (#202011159154) and the HKU 45th round PDF scheme. For use of the PhenoCam data, we thank our many collaborators, including site PIs and technicians, for their efforts in support of PhenoCam. The development of PhenoCam has been funded by the Northeastern States Research Cooperative, NSF's Macrosystems Biology program (awards EF-1065029 and EF-1702697), and DOE's Regional and Global Climate Modelling program (award DE-SC0016011). We acknowledge additional support from the US National Park Service Inventory and Monitoring Program and the USA National Phenology Network (grant number G10AP00129 from the United States Geological Survey), and from the USA National Phenology Network and North Central Climate Science Center (cooperative agreement number G16AC00224 from the United States Geological Survey). Additional funding, through the National Science Foundation's LTER program, has supported research at Harvard Forest (DEB-1237491) and Bartlett Experimental Forest (DEB-1114804). We also thank the USDA Forest Service Air Resource Management program and the National Park Service Air Resources program for contributing their camera imagery to the PhenoCam archive.

## Appendix A. Supplementary data

Supplementary data to this article can be found online at <https://doi.org/10.1016/j.rse.2023.113617>.

## References

- Ashcroft, G., Richardson, E., Seeley, S., Walker, D., Anderson, J., Griffin, R., Alfaro, J., Keller, J., 1974. Use of fruit bud climatography to program sprinkling for bloom delay. In: ASAE Paper No. PNW 74-22, ASAE, St. Joseph, MI, 49085.
- Badeck, F.-W., Bondeau, A., Böttcher, K., Doktor, D., Lucht, W., Schaber, J., Sitch, S., 2004. Responses of spring phenology to climate change. *New Phytol.* 162, 295–309.
- Basler, D., 2016. Evaluating phenological models for the prediction of leaf-out dates in six temperate tree species across Central Europe. *Agric. For. Meteorol.* 217, 10–21.
- Bennie, J., Kubin, E., Wiltshire, A., Huntley, B., Baxter, R., 2010. Predicting spatial and temporal patterns of bud-burst and spring frost risk in north-West Europe: the implications of local adaptation to climate. *Glob. Chang. Biol.* 16, 1503–1514.
- Bolton, D.K., Gray, J.M., Melaas, E.K., Moon, M., Eklundh, L., Friedl, M.A., 2020. Continental-scale land surface phenology from harmonized landsat 8 and sentinel-2 imagery. *Remote Sens. Environ.* 240, 111685.
- Bozdogan, H., 1987. Model selection and Akaike's information criterion (AIC): the general theory and its analytical extensions. *Psychometrika* 52, 345–370.
- Brown, T.B., Hultine, K.R., Steltzer, H., Denny, E.G., Denslow, M.W., Granados, J., Henderson, S., Moore, D., Nagai, S., SanClemente, M., 2016. Using phenocams to monitor our changing earth: toward a global phenocam network. *Front. Ecol. Environ.* 14, 84–93.
- Caffarra, A., Donnelly, A., Chuine, I., 2011. Modelling the timing of *Betula pubescens* budburst II. Integrating complex effects of photoperiod into process-based models. *Clim. Res.* 46, 159–170.
- Cannell, M., Smith, R., 1983. Thermal time, chill days and prediction of budburst in *Picea sitchensis*. *J. Appl. Ecol.* 951–963.
- Caparros-Santiago, J.A., Rodriguez-Galiano, V., Dash, J., 2021. Land surface phenology as indicator of global terrestrial ecosystem dynamics: a systematic review. *ISPRS J. Photogramm. Remote Sens.* 171, 330–347.
- Chmura, H.E., Kharouba, H.M., Ashander, J., Ehlm, S.M., Rivest, E.B., Yang, L.H., 2019. The mechanisms of phenology: the patterns and processes of phenological shifts. *Ecol. Monogr.* 89, e01337.
- Chuine, I., Bonhomme, M., Legave, J.M., García de Cortázar-Atauri, I., Charrier, G., Lacointe, A., Améglio, T., 2016. Can phenological models predict tree phenology accurately in the future? The unrevealed hurdle of endodormancy break. *Glob. Chang. Biol.* 22, 3444–3460.
- Cleland, E.E., Chiariello, N.R., Loarie, S.R., Mooney, H.A., Field, C.B., 2006. Diverse responses of phenology to global changes in a grassland ecosystem. *Proc. Natl. Acad. Sci.* 103, 13740–13744.
- Dai, W., Jin, H., Zhang, Y., Liu, T., Zhou, Z., 2019. Detecting temporal changes in the temperature sensitivity of spring phenology with global warming: application of machine learning in phenological model. *Agric. For. Meteorol.* 279, 107702.
- De Réaumur, R., 1735. Observations du thermomètre. In: *Memories Académie Royale Sciences Paris*, pp. 545–576.
- Delpierre, N., Berveiller, D., Granda, E., Dufrêne, E., 2016. Wood phenology, not carbon input, controls the interannual variability of wood growth in a temperate oak forest. *New Phytol.* 210, 459–470.
- Descals, A., Verger, A., Yin, G., Filella, I., Fu, Y.H., Piao, S., Janssens, I.A., Peñuelas, J., 2022. Radiation-constrained boundaries cause nonuniform responses of the carbon uptake phenology to climatic warming in the northern hemisphere. *Glob. Chang. Biol.* 29, 719–730.
- Dong, T., Shang, J., Qian, B., Liu, J., Chen, J.M., Jing, Q., McConkey, B., Huffman, T., Daneshfar, B., Champagne, C., Davidson, A., MacDonald, D., 2019. Field-Scale Crop Seeding Date Estimation from MODIS Data and Growing Degree Days in Manitoba, Canada. *Remote Sens.* 11, 1760.
- Donnelly, A., Yu, R., Caffarra, A., Hanes, J., Liang, L., Desai, A.R., Liu, L., Schwartz, M.D., 2017. Interspecific and interannual variation in the duration of spring phenophases in a northern mixed forest. *Agric. For. Meteorol.* 243, 55–67.
- Durand, M., Murchie, E.H., Lindfors, A.V., Urban, O., Aphalo, P.J., Robson, T.M., 2021. Diffuse solar radiation and canopy photosynthesis in a changing environment. *Agric. For. Meteorol.* 311, 108684.
- Elmore, A.J., Guinn, S.M., Minsley, B.J., Richardson, A.D., 2012. Landscape controls on the timing of spring, autumn, and growing season length in mid-Atlantic forests. *Glob. Chang. Biol.* 18, 656–674.
- Estrella, N., Heinemann, V., Menzel, A., 2017. In: *Frost sensitivity of various deciduous plant species during leaf development in spring*, p. 8416.
- Farquhar, G.D., von Caemmerer, S., Berry, J.A., 1980. A biochemical model of photosynthetic CO<sub>2</sub> assimilation in leaves of C3 species. *Planta* 149, 78–90.
- Felton, A.J., Slette, J.J., Smith, M.D., Knapp, A.K., 2020. Precipitation amount and event size interact to reduce ecosystem functioning during dry years in a Meso grassland. *Glob. Chang. Biol.* 26, 658–668.
- Fernandez, E., Schifflers, K., Urbach, C., Luedeling, E., 2022. Unusually warm winter seasons may compromise the performance of current phenology models—Predicting bloom dates in young apple trees with PhenoFlex. *Agric. For. Meteorol.* 322, 109020.
- Fisher, J.I., Richardson, A.D., Mustard, J.F., 2007. Phenology model from surface meteorology does not capture satellite-based Greenup estimations. *Glob. Chang. Biol.* 13, 707–721.
- Flynn, D.F.B., Wolkovich, E.M., 2018. Temperature and photoperiod drive spring phenology across all species in a temperate forest community. *New Phytol.* 219, 1353–1362.
- Friedl, M., Gray, J., Sulla-Menashe, D., 2019. MCD12Q2 MODIS/Terra+ aqua land cover dynamics yearly L3 global 500m SIN grid V006. NASA EOSDIS land processes DAAC.
- Fu, X., Wang, J., Wang, H., Dai, X., Yang, F., Zhao, M., 2016. Response of the fine root production, phenology, and turnover rate of six shrub species from a subtropical forest to a soil moisture gradient and shading. *Plant Soil* 399, 135–146.
- Fu, Y.H., Zhang, X., Piao, S., Hao, F., Geng, X., Vitasse, Y., Zohner, C., Peñuelas, J., Janssens, I.A., 2019. Daylength helps temperate deciduous trees to leaf-out at the optimal time. *Glob. Chang. Biol.* 25, 2410–2418.
- Fu, Y.H., Zhao, H., Piao, S., Peaucelle, M., Peng, S., Zhou, G., Ciais, P., Huang, M., Menzel, A., Peñuelas, J., Song, Y., Vitasse, Y., Zeng, Z., Janssens, I.A., 2015. Declining global warming effects on the phenology of spring leaf unfolding. *Nature* 526, 104–107.
- Fu, Y.H., Zhou, X., Li, X., Zhang, Y., Geng, X., Hao, F., Zhang, X., Hanninen, H., Guo, Y., De Boeck, H.J., 2021. Decreasing control of precipitation on grassland spring phenology in temperate China. *Glob. Ecol. Biogeogr.* 30, 490–499.
- Galvagno, M., Wohlfahrt, G., Cremonese, E., Rossini, M., Colombo, R., Filippa, G., Julitta, T., Manca, G., Siniscalco, C., Di Celli, U.M., 2013. Phenology and carbon dioxide source/sink strength of a subalpine grassland in response to an exceptionally short snow season. *Environ. Res. Lett.* 8, 025008.
- Gao, M., Piao, S., Chen, A., Yang, H., Liu, Q., Fu, Y.H., Janssens, I.A., 2019. Divergent changes in the elevational gradient of vegetation activities over the last 30 years. *Nat. Commun.* 10, 2970.
- Gonsamo, A., Chen, J.M., 2016. Circumpolar vegetation dynamics product for global change study. *Remote Sens. Environ.* 182, 13–26.
- Hänen, H., Kramer, K., Tanino, K., Zhang, R., Wu, J., Fu, Y.H., 2019. Experiments are necessary in process-based tree phenology modelling. *Trends in Plant Science* 24, 199–209.
- Herrmann, H.A., Schwartz, J.-M., Johnson, G.N., 2020. From empirical to theoretical models of light response curves - linking photosynthetic and metabolic acclimation. *Photosynth. Res.* 145, 5–14.
- Huang, W., Ge, Q., Wang, H., Dai, J., 2019. Effects of multiple climate change factors on the spring phenology of herbaceous plants in Inner Mongolia, China: evidence from ground observation and controlled experiments. *Int. J. Climatol.* 39, 5140–5153.
- Hufkens, K., Basler, D., Milliman, T., Melaas, E.K., Richardson, A.D., 2018. An integrated phenology modelling framework in r. *Methods Ecol. Evol.* 9, 1276–1285.
- Hwang, T., Song, C., Vose, J.M., Band, L.E., 2011. Topography-mediated controls on local vegetation phenology estimated from MODIS vegetation index. *Landscape Ecol.* 26, 541–556.
- Johnson, I., Thornley, J., 1985. Temperature dependence of plant and crop process. *Ann. Bot.* 55, 1–24.
- Jumrani, K., Bhatia, V.S., 2020. Influence of different light intensities on specific leaf weight, stomatal densities photosynthesis and seed yield in soybean. *Plant Physiol. Reports* 25, 277–283.
- Kim, S., Kim, T.K., Yoon, S., Jang, K., Chun, J.-H., Won, M., Lim, J.-H., Kim, H.S., 2022. Quantifying the importance of day length in process-based models for the prediction of temperate spring flowering phenology. *Sci. Total Environ.* 843, 156780.
- Körner, C., 2006. Significance of temperature in plant life. In: *Plant Growth and Climate Change*, pp. 48–69.
- Körner, C., Basler, D., 2010. Phenology under global warming. *Science* 327, 1461–1462.
- Lee, B.R., Ibáñez, I., 2021. Spring phenological escape is critical for the survival of temperate tree seedlings. *Funct. Ecol.* 35, 1848–1861.
- Li, X., Zhang, L., Luo, T., 2020. Rainy season onset mainly drives the spatiotemporal variability of spring vegetation green-up across alpine dry ecosystems on the tibetan plateau. *Sci. Rep.* 10, 1–10.
- Lian, X., Piao, S., Li, L.Z., Li, Y., Huntingford, C., Ciais, P., Cescatti, A., Janssens, I.A., Peñuelas, J., Buermann, W., 2020. Summer soil drying exacerbated by earlier spring greening of northern vegetation. *Sci. Adv.* 6 eaax0255.
- Lin, X., Wu, S., Chen, B., Lin, Z., Yan, Z., Chen, X., Yin, G., You, D., Wen, J., Liu, Q., 2022. Estimating 10-m land surface albedo from Sentinel-2 satellite observations using a direct estimation approach with Google earth engine. *ISPRS J. Photogramm. Remote Sens.* 194, 1–20.
- Liu, L., Liang, L., Schwartz, M.D., Donnelly, A., Wang, Z., Schaaf, C.B., Liu, L., 2015. Evaluating the potential of MODIS satellite data to track temporal dynamics of autumn phenology in a temperate mixed forest. *Remote Sens. Environ.* 160, 156–165.
- Liu, Y., Reich, P.B., Li, G., Sun, S., 2011. Shifting phenology and abundance under experimental warming alters trophic relationships and plant reproductive capacity. *Ecology* 92, 1201–1207.
- Lundell, R., Hänen, H., Saarinen, T., Åström, H., Zhang, R., 2020. Beyond rest and quiescence (endodormancy and ecodormancy): a novel model for quantifying plant-environment interaction in bud dormancy release. *Plant Cell Environ.* 43, 40–54.
- Ma, Q., Huang, J.G., Hänen, H., Li, X., Berninger, F., 2021. Climate warming prolongs the time interval between leaf-out and flowering in temperate trees: effects of chilling, forcing and photoperiod. *J. Ecol.* 109, 1319–1330.
- Ma, X., Zhu, X., Xie, Q., Jin, J., Zhou, Y., Luo, Y., Liu, Y., Tian, J., Zhao, Y., 2022. Monitoring nature's calendar from space: Emerging topics in land surface phenology and associated opportunities for science applications. *Glob. Chang. Biol.* 28, 7186–7204.
- Mäkiranta, P., Laiho, R., Mehtätalo, L., Straková, P., Sormunen, J., Minkkinen, K., Penttilä, T., Fritze, H., Tuittila, E.S., 2018. Responses of phenology and biomass production of boreal fens to climate warming under different water-table level regimes. *Glob. Chang. Biol.* 24, 944–956.

- Marchand, L.J., Dox, I., Gričar, J., Prislan, P., Leys, S., Van den Bulcke, J., Fonti, P., Lange, H., Matthysen, E., Peñuelas, J., Zuccarini, P., Campioli, M., 2020. Inter-individual variability in spring phenology of temperate deciduous trees depends on species, tree size and previous year autumn phenology. *Agric. For. Meteorol.* 290, 108031.
- McMahon, G., Gregonis, S.M., Waltman, S.W., Omernik, J.M., Thorson, T.D., Freeouf, J.A., Rorick, A.H., Keys, J.E., 2001. Developing a spatial framework of common ecological regions for the conterminous United States. *Environ. Manag.* 28, 293–316.
- Medlyn, B.E., Dreyer, E., Ellsworth, D., Forstreuter, M., Harley, P.C., Kirschbaum, M.U.F., Le Roux, X., Montpied, P., Strassmeyer, J., Walcroft, A., Wang, K., Loustau, D., 2002. Temperature response of parameters of a biochemically based model of photosynthesis. II. A review of experimental data. *Plant Cell Environ.* 25, 1167–1179.
- Meng, L., 2021. Green with phenology. *Science* 374, 1065–1066.
- Meng, L., Mao, J., Ricciuto, D.M., Shi, X., Richardson, A.D., Hanson, P.J., Warren, J.M., Zhou, Y., Li, X., Zhang, L., Schädel, C., 2021a. Evaluation and modification of ELM seasonal deciduous phenology against observations in a southern boreal peatland forest. *Agric. For. Meteorol.* 308–309, 108556.
- Meng, L., Zhou, Y., Gu, L., Richardson, A.D., Peñuelas, J., Fu, Y., Wang, Y., Asrar, G.R., De Boeck, H.J., Mao, J., Zhang, Y., Wang, Z., 2021b. Photoperiod decelerates the advance of spring phenology of six deciduous tree species under climate warming. *Glob. Chang. Biol.* 27, 2914–2927.
- Migliavacca, M., Galvagno, M., Cremonese, E., Rossini, M., Meroni, M., Sonnentag, O., Cogliati, S., Manca, G., Diotri, F., Busetto, L., Cescatti, A., Colombo, R., Fava, F., Morra di Cella, U., Pari, E., Siniscalco, C., Richardson, A.D., 2011. Using digital repeat photography and eddy covariance data to model grassland phenology and photosynthetic CO<sub>2</sub> uptake. *Agric. For. Meteorol.* 151, 1325–1337.
- Moon, M., Richardson, A.D., Friedl, M.A., 2021a. Multiscale assessment of land surface phenology from harmonized landsat 8 and Sentinel-2, PlanetScope, and PhenoCam imagery. *Remote Sens. Environ.* 266, 112716.
- Moon, M., Richardson, A.D., Milliman, T., Friedl, M.A., 2022. A high spatial resolution land surface phenology dataset for AmeriFlux and NEON sites. *Sci. Data* 9, 448.
- Moon, M., Seyednasrollah, B., Richardson, A.D., Friedl, M.A., 2021b. Using time series of MODIS land surface phenology to model temperature and photoperiod controls on spring Greenup in north american deciduous forests. *Remote Sens. Environ.* 260, 112466.
- Omernik, J.M., 1987. Ecoregions of the conterminous United States. *Ann. Assoc. Am. Geogr.* 77, 118–125.
- Osvalainen, O., Skorokhodova, S., Yakovleva, M., Sukhov, A., Kutenkov, A., Kutenkova, N., Shcherbakov, A., Meyke, E., Delgado, M.D.M., 2013. Community-level phenological response to climate change. *Proc. Natl. Acad. Sci.* 110, 13434–13439.
- Peng, D., Zhang, X., Wu, C., Huang, W., Gonsamo, A., Huete, A.R., Didan, K., Tan, B., Liu, X., Zhang, B., 2017. Intercomparison and evaluation of spring phenology products using National Phenology Network and AmeriFlux observations in the contiguous United States. *Agric. For. Meteorol.* 242, 33–46.
- Peng, J., Wu, C., Wang, X., Lu, L., 2021. Spring phenology outweighed climate change in determining autumn phenology on the tibetan plateau. *Int. J. Climatol.* 41, 3725–3742.
- Piao, S., Liu, Q., Chen, A., Janssens, I.A., Fu, Y., Dai, J., Liu, L., Lian, X., Shen, M., Zhu, X., 2019. Plant phenology and global climate change: current progresses and challenges. *Glob. Chang. Biol.* 25, 1922–1940.
- Piao, S., Wang, J., Li, X., Xu, H., Zhang, Y., 2022. Spatio-temporal changes in the speed of canopy development and senescence in temperate China. *Glob. Chang. Biol.* 28, 7366–7375.
- Post, A.K., Hufkens, K., Richardson, A.D., 2022. Predicting spring green-up across diverse north american grasslands. *Agric. For. Meteorol.* 327, 109204.
- Ren, S., Peichl, M., 2021. Enhanced spatiotemporal heterogeneity and the climatic and biotic controls of autumn phenology in northern grasslands. *Sci. Total Environ.* 788, 147806.
- Richardson, A.D., Hufkens, K., Milliman, T., Aubrecht, D.M., Chen, M., Gray, J.M., Johnston, M.R., Keenan, T.F., Klosterman, S.T., Kosmala, M., 2018a. Tracking vegetation phenology across diverse north american biomes using PhenoCam imagery. *Sci. Data* 5, 1–24.
- Richardson, A.D., Hufkens, K., Milliman, T., Aubrecht, D.M., Furze, M.E., Seyednasrollah, B., Krassovski, M.B., Latimer, J.M., Nettles, W.R., Heiderman, R.R., 2018b. Ecosystem warming extends vegetation activity but heightens vulnerability to cold temperatures. *Nature* 560, 368–371.
- Richardson, A.D., Hufkens, K., Milliman, T., Frolking, S., 2018c. Intercomparison of phenological transition dates derived from the PhenoCam dataset V1. 0 and MODIS satellite remote sensing. *Sci. Rep.* 8, 1–12.
- Richardson, A.D., Keenan, T.F., Migliavacca, M., Ryu, Y., Sonnentag, O., Toomey, M., 2013. Climate change, phenology, and phenological control of vegetation feedbacks to the climate system. *Agric. For. Meteorol.* 169, 156–173.
- Roberts, A.M.I., Tansey, C., Smithers, R.J., Phillipmore, A.B., 2015. Predicting a change in the order of spring phenology in temperate forests. *Glob. Chang. Biol.* 21, 2603–2611.
- Savage, J.A., Chuique, I., 2021. Coordination of spring vascular and organ phenology in deciduous angiosperms growing in seasonally cold climates. *New Phytol.* 230, 1700–1715.
- Schwartz, M.D., Hanes, J.M., 2010. Continental-scale phenology: warming and chilling. *Int. J. Climatol.* 30, 1595–1598.
- Seyednasrollah, B., Young, A.M., Hufkens, K., Milliman, T., Friedl, M.A., Frolking, S., Richardson, A.D., 2019. Tracking vegetation phenology across diverse biomes using version 2.0 of the PhenoCam dataset. *Sci. Data* 6, 1–11.
- Shen, M., Wang, S., Jiang, N., Sun, J., Cao, R., Ling, X., Fang, B., Zhang, L., Zhang, L., Xu, X., Lv, W., Li, B., Sun, Q., Meng, F., Jiang, Y., Dorji, T., Fu, Y., Iler, A., Vitasse, Y., Steltzer, H., Ji, Z., Zhao, W., Piao, S., Fu, B., 2022. Plant phenology changes and drivers on the Qinghai-tibetan plateau. *Nat. Rev. Earth Environ.* 3, 633–651.
- Singh, R.K., Svystun, T., AlDahmash, B., Jönsson, A.M., Bhalerao, R.P., 2017. Photoperiod-and temperature-mediated control of phenology in trees—a molecular perspective. *New Phytol.* 213, 511–524.
- Stone, M., 1977. An asymptotic equivalence of choice of model by cross-validation and Akaike's criterion. *J. R. Stat. Soc. Ser. B Methodol.* 39, 44–47.
- Sun, J., Liu, B., You, Y., Li, W., Liu, M., Shang, H., He, J.-S., 2019. Solar radiation regulates the leaf nitrogen and phosphorus stoichiometry across alpine meadows of the tibetan plateau. *Agric. For. Meteorol.* 271, 92–101.
- Tang, J., Körner, C., Muraroaka, H., Piao, S., Shen, M., Thackeray, S.J., Yang, X., 2016. Emerging opportunities and challenges in phenology: a review. *Ecosphere* 7, e01436.
- Tao, Z., Ge, Q., Wang, H., Dai, J., 2020a. The important role of soil moisture in controlling autumn phenology of herbaceous plants in the inner mongolian steppe. *Land Degrad. Dev.* 32.
- Tao, Z., Huang, W., Wang, H., 2020b. Soil moisture outweighs temperature for triggering the green-up date in temperate grasslands. *Theor. Appl. Climatol.* 140, 1093–1105.
- Thornton, M., Thornton, P., Wei, Y., Vose, R.A., Boyer, A., 2017. Daymet: Station-level inputs and model predicted values for North America, Version 3. ORNL DAAC.
- Thornton, P., Thornton, M., Mayer, B., Wei, Y., Devarakonda, R., Vose, R., Cook, R., 2016. Daymet: Daily Surface Weather Data on a 1-km Grid for North America, Version 3. ORNL DAAC, Oak Ridge, Tennessee, USA.
- Thornton, P.E., Shrestha, R., Thornton, M., Kao, S.-C., Wei, Y., Wilson, B.E., 2021. Gridded daily weather data for North America with comprehensive uncertainty quantification. *Sci. Data* 8, 190.
- Tumajer, J., Buras, A., Camarero, J.J., Carrer, M., Shetti, R., Wilmking, M., Altman, J., Sangüesa-Barreda, G., Lehejček, J., 2021. Growing faster, longer or both? Modelling plastic response of *Juniperus communis* growth phenology to climate change. *Glob. Ecol. Biogeogr.* 30, 2229–2244.
- Viherä-Aarnio, A., Sutinen, S., Partanen, J., Häkkinen, R., 2014. Internal development of vegetative buds of Norway spruce trees in relation to accumulated chilling and forcing temperatures. *Tree Physiol.* 34, 547–556.
- Viswanathan, M., Weber, T.K.D., Gayler, S., Mai, J., Streck, T., 2022. A bayesian sequential updating approach to predict phenology of silage maize. *Biogeosciences* 19, 2187–2209.
- Vitasse, Y., François, C., Delpierre, N., Dufrêne, E., Kremer, A., Chuique, I., Delzon, S., 2011. Assessing the effects of climate change on the phenology of european temperate trees. *Agric. For. Meteorol.* 151, 969–980.
- Vitasse, Y., Signarbeaux, C., Fu, Y.H., 2018. Global warming leads to more uniform spring phenology across elevations. *Proc. Natl. Acad. Sci.* 115, 1004–1008.
- Wang, H., Dai, J., Peñuelas, J., Ge, Q., Fu, Y.H., Wu, C., 2022. Winter warming offsets one half of the spring warming effects on leaf unfolding. *Glob. Chang. Biol.* 28, 6033–6049.
- Wang, H., Liu, H., Cao, G., Ma, Z., Li, Y., Zhang, F., Zhao, X., Zhao, X., Jiang, L., Sanders, N.J., Classen, A.T., He, J.-S., 2020a. Alpine grassland plants grow earlier and faster but biomass remains unchanged over 35 years of climate change. *Ecol. Lett.* 23, 701–710.
- Wang, H., Wu, C., Ciais, P., Peñuelas, J., Dai, J., Fu, Y., Ge, Q., 2020. Overestimation of the effect of climatic warming on spring phenology due to misrepresentation of chilling. *Nat. Commun.* 11.
- Wang, J., Xi, Z., He, X., Chen, S., Rossi, S., Smith, N.G., Liu, J., Chen, L., 2021. Contrasting temporal variations in responses of leaf unfolding to daytime and nighttime warming. *Glob. Chang. Biol.* 27, 5084–5093.
- Way, D.A., Montgomery, R.A., 2015. Photoperiod constraints on tree phenology, performance and migration in a warming world. *Plant Cell Environ.* 38, 1725–1736.
- Wu, C., Peng, J., Ciais, P., Peñuelas, J., Wang, H., Beguería, S., Andrew Black, T., Jassal, R.S., Zhang, X., Yuan, W., Liang, E., Wang, X., Hua, H., Liu, R., Ju, W., Fu, Y., H., Ge, Q., 2022. Increased drought effects on the phenology of autumn leaf senescence. *Nat. Clim. Chang.* 12, 943–949.
- Xin, Q., Broich, M., Zhu, P., Gong, P., 2015. Modeling grassland spring onset across the Western United States using climate variables and MODIS-derived phenology metrics. *Remote Sens. Environ.* 161, 63–77.
- Xu, X., Medvigy, D., Joseph Wright, S., Kitajima, K., Wu, J., Albert, L.P., Martins, G.A., Saleska, S.R., Pacala, S.W., 2017. Variations of leaf longevity in tropical moist forests predicted by a trait-driven carbon optimality model. *Ecol. Lett.* 20, 1097–1106.
- Yang, Y., Chen, R., Yin, G., Wang, C., Liu, G., Verger, A., Descals, A., Filella, I., Peñuelas, J., 2022. Divergent performances of vegetation indices in extracting photosynthetic phenology for northern deciduous broadleaf forests. *IEEE Geosci. Remote Sens. Lett.* 19, 1–5.
- Yao, Y., Vehtari, A., Simpson, D., Gelman, A., 2018. Using stacking to average bayesian predictive distributions (with Discussion). *Bayesian Anal.* 13 (917–1007), 1091.
- Yun, J., Jeong, S.-J., Ho, C.-H., Park, C.-E., Park, H., Kim, J., 2018. Influence of winter precipitation on spring phenology in boreal forests. *Glob. Chang. Biol.* 24, 5176–5187.
- Zanaga, D., Van de Kerchove, R., Daems, D., De Keersmaecker, W., Brockmann, C., Kirches, G., Wevers, J., Cartus, O., Santoro, M., Fritz, S., 2022. ESA WorldCover 10 m 2021 v200.
- Zhang, H., Liu, S., Regnier, P., Yuan, W., 2018. New insights on plant phenological response to temperature revealed from long-term widespread observations in China. *Glob. Chang. Biol.* 24, 2066–2078.
- Zhang, X., Friedl, M., Henebry, G., 2020a. VIIRS/NPP land cover dynamics yearly L3 global 500m SIN grid V001. NASA EOSDIS Land Processes DAAC.

- Zhang, X., Wang, J., Gao, F., Liu, Y., Schaaf, C., Friedl, M., Yu, Y., Jayavelu, S., Gray, J., Liu, L., 2017. Exploration of scaling effects on coarse resolution land surface phenology. *Remote Sens. Environ.* 190, 318–330.
- Zhang, Y., Commane, R., Zhou, S., Williams, A.P., Gentile, P., 2020b. Light limitation regulates the response of autumn terrestrial carbon uptake to warming. *Nat. Clim. Chang.* 10, 739–743.
- Zhao, H., Fu, Y.H., Wang, X., Zhang, Y., Liu, Y., Janssens, I.A., 2021. Diverging models introduce large uncertainty in future climate warming impact on spring phenology of temperate deciduous trees. *Sci. Total Environ.* 757, 143903.
- Zhao, Y., Lee, C.K.F., Wang, Z., Wang, J., Gu, Y., Xie, J., Law, Y.K., Song, G., Bonebrake, T.C., Yang, X., Nelson, B.W., Wu, J., 2022. Evaluating fine-scale phenology from PlanetScope satellites with ground observations across temperate forests in eastern North America. *Remote Sens. Environ.* 283, 113310.
- Zhou, G., Wang, Q., 2018. A new nonlinear method for calculating growing degree days. *Sci. Rep.* 8, 10149.
- Zohner, C.M., Benito, B.M., Svenning, J.-C., Renner, S.S., 2016. Day length unlikely to constrain climate-driven shifts in leaf-out times of northern woody plants. *Nat. Clim. Chang.* 6, 1120–1123.
- Zohner, C.M., Mo, L., Pugh, T.A.M., Bastin, J.-F., Crowther, T.W., 2020a. Interactive climate factors restrict future increases in spring productivity of temperate and boreal trees. *Glob. Chang. Biol.* 26, 4042–4055.
- Zohner, C.M., Mo, L., Renner, S.S., Svenning, J.-C., Vitasse, Y., Benito, B.M., Ordóñez, A., Baumgarten, F., Bastin, J.-F., Sebald, V., Reich, P.B., Liang, J., Nabuurs, G.-J., De-Miguel, S., Alberti, G., Antón-Fernández, C., Balazy, R., Brändli, U.-B., Chen, H.Y.H., Chisholm, C., Cienciala, E., Dayanandan, S., Fayle, T.M., Frizzera, L., Gianelle, D., Jagodzinski, A.M., Jaroszewicz, B., Jucker, T., Kepfer-Rojas, S., Khan, M.L., Kim, H. S., Korjus, H., Johannsen, V.K., Laarmann, D., Lang, M., Zawila-Niedzwiecki, T., Niklaus, P.A., Paquette, A., Pretzsch, H., Saikia, P., Schall, P., Šeben, V., Svoboda, M., Tikhonova, E., Viana, H., Zhang, C., Zhao, X., Crowther, T.W., 2020b. Late-spring frost risk between 1959 and 2017 decreased in North America but increased in Europe and Asia. *Proc. Natl. Acad. Sci.* 117, 12192–12200.
- Zohner, C.M., Mo, L., Sebald, V., Renner, S.S., 2020c. Leaf-out in northern ecotypes of wide-ranging trees requires less spring warming, enhancing the risk of spring frost damage at cold range limits. *Glob. Ecol. Biogeogr.* 29, 1065–1072.